

A Project Report entitled

Development of MEMS based Micropumps for Medical Applications

Submitted by

SHIRSHENDU CHATTERJEE

University Registration Number: D01-1111-0066-18

Examination Roll Number: T91/ECE/184068

Under the Supervision of

Dr. ANIRBAN BHATTACHARYYA

Assistant Professor

Department of Radiophysics and Electronics

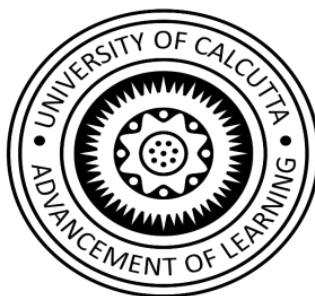
University of Calcutta

For the partial fulfillment of the degree of

Bachelor of Technology

In

Electronics and Communication Engineering



Department of Radiophysics and Electronics,
University College of Science and Technology,
University of Calcutta
92, Acharya Prafulla Chandra Road,
Kolkata – 7000 009



University

of Calcutta

UNIVERSITY COLLEGE OF TECHNOLOGY

INSTITUTE OF RADIOPHYSICS AND ELECTRONICS

Telephone: (+91)(33)2350-9115/9116/9413
Telegram : INRAPHEL
Fax : (+91)(33)2351-5828
Email : anirban1@gmail.com
Website : www.irpel.org

SISIR MITRA BHAVAN
92, Acharya Prafulla Chandra Road
Kolkata-700009, INDIA

CERTIFICATE

This is to certify that **Shirshendu Chatterjee (Registration Number- D01-1111-0066-18, Roll No. T91/ECE/184068)** student of B.Tech 8th Semester, Department of Radiophysics and Electronics, University of Calcutta have pursued their B.Tech project "**Development of MEMS based Micropumps for Medical Applications**" for degree of Bachelor of Technology in Electronics and Communication Engineering under my guidance and supervision. This project is completed in accordance with department's issued guidelines.

Dr. Anirban Bhattacharyya.

Assistant Professor.

Institute of Radiophysics
& Electronics.

University of Calcutta.

Date:

ACKNOWLEDGEMENTS

Firstly, I would like to express our sincere gratitude to our supervisor Dr. Anirban Bhattacharyya of the Institute of Radiophysics and Electronics, University of Calcutta for his guidance, supervision, and inspiration in initiating the project, laying the building blocks and the successful completion of the project.

I would like to thank our Head of the Department Dr. Abhijit Biswas for encouraging us to work on this project.

I would like to thank our scholars, batchmates and seniors of the Department of Radiophysics and Electronics for their valuable suggestions and kind cooperation to us.

Lastly, I would like to express spate of gratitude to the Institute of Radio physics and Electronics (C.U.) for allowing me to work for successful completion of this project.

SHIRSHENDU CHATTERJEE

PREFACE

We have had immense pleasure in working on this project. Micropumps that are developed serves as potential devices for treatment of chronic diseases in the bio-medical domain.

By having an opportunity to work on this project we are very much glad. Some difficulties arose as we were in our home for doing this project due to the present pandemic situation and could not meet with each other. But our hard work and cooperation were able to partially complete this project successfully.

We are grateful to our classmates, who helped us by giving various information and gave constant support and encouragement. We offer our deep sense of gratitude to our guide, professor of the department of Radio Physics and Electronics. Our special thanks to our family members, our teammates, and our department.

SHIRSHENDU CHATTERJEE

ABSTRACT

With the proliferation of technologies, treatments for various diseases have been elevated in the recent years. Such technologies and frameworks also include the application of Micro-Electro-Mechanical-Systems (MEMS) in bio-medical domains. MEMS based micropumps has been used in several applications of drug-delivery, DNA hybridization etc. In this project, applications of micropumps in Wound Therapy and treatment of Glaucoma is presented. Complying with the classical Negative Pressure Wound Therapy (NPWT), nozzle/diffuser micropumps have been used to use as smart band-aid system to cover wounds outside skin as well as for in-vitro applications. Another aspect of medical treatment this project focuses on is the application of micropump for the treatment of Intraocular Pressure (IOP) or Glaucoma. Glaucoma serves as the main problem for increase in eye pressure or intraocular pressure. The project focuses on design and development of a device - peristaltic micropump with integrated piezoelectric pressure sensor, which self-actuates due to applied pressure on the piezoelectric membrane and pumps out the fluid out of the eye to lower the pressure. The idea and devices developed are state-of-art devices and can be potential devices for such treatments as no such devices has been designed or developed till now.

Contents

| | |
|--|----|
| Contents..... | 1 |
| List of Figures..... | 3 |
| 1. Introduction..... | 6 |
| 1.1. Motivation..... | 8 |
| 1.2. Wound Therapy..... | 9 |
| 1.2.1 Functional Principle of NPWT..... | 9 |
| 1.2.2 Mechanism of action of NPWT..... | 9 |
| 1.2.3 Treatment and the Scientific Background..... | 11 |
| 1.3. Intraocular Pressure (IOP) / Glaucoma..... | 15 |
| 1.3.1 Standard Techniques for IOP Measurement..... | 18 |
| 1.3.1.1 Applanation (Goldmann) Tonometry..... | 18 |
| 1.3.1.2 Non-contact Tonometry (Pneumotonometry)..... | 19 |
| 1.3.2 Need for continuous IOP measurement..... | 19 |
| 1.4 Thesis Outline..... | 20 |
| References..... | 21 |
| 2. MEMS Micropumps..... | 24 |
| 2.1 Actuation Principles..... | 24 |
| 2.1.1 Piezoelectric Sensing and Actuation..... | 25 |
| 2.1.2 Mathematical description of Piezoelectric Effects..... | 27 |
| 2.2 Valveless Micropumps..... | 31 |
| 2.2.1 Principle of Operation..... | 31 |
| 2.2.1.1 Nozzle/Diffuser Elements..... | 32 |
| 2.2.1.2 Theoretical Analysis..... | 33 |
| 2.3 Peristaltic Micropumps..... | 39 |
| 2.3.1 Pump Design..... | 40 |
| 2.3.2 Pumping Cell Representation..... | 40 |
| 2.3.2.1 Diaphragm Vibrations..... | 41 |
| 2.3.2.2 Fluid Flow..... | 43 |

| | |
|---|-----------|
| 2.3.3 System-level pump model..... | 45 |
| References..... | 46 |
| 3. Concept for Application of Micropumps | 52 |
| 3.1 Application of Nozzle/Diffuser Micropump in NPWT..... | 52 |
| 3.2 Application of Peristaltic Micropump with incorporated pressure sensor for treatment of Glaucoma..... | 53 |
| References..... | 54 |
| 4. Simulation and Results..... | 55 |
| 4.1 Nozzle/Diffuser Micropump for NPWT..... | 55 |
| 4.1.1 Design and Geometry..... | 56 |
| 4.1.2 Boundary Conditions..... | 58 |
| 4.1.3 Mesh Formation..... | 60 |
| 4.2 Results..... | 62 |
| 4.3 Peristaltic Micropump for Glaucoma..... | 75 |
| 5. Summary and Conclusion..... | 76 |
| 6. Future Scope..... | 78 |

List of Figures

| | |
|---|----|
| 1-1 Principle of Negative Pressure Wound Therapy..... | 9 |
| 1-2 Different types of Wounds in NPWT..... | 14 |
| 1-3 (a) Structure of the Human Eye (b) Distinct description of the eye from where aqueous humor flows..... | 15 |
| 1-4 Schematic diagram illustrating the trabecular meshwork..... | 16 |
| 1-5 Open angle and angle-closure glaucoma..... | 17 |
| 2-1 A schematic figure of the transfer of input energy to output work in an actuator..... | 25 |
| 2-2 Schematic illustration of piezoelectric crystal in a rectangular system..... | 27 |
| 2-3 The deformation of piezoelectric device when subject to electrical voltage..... | 28 |
| 2-4 The bending of a bimorph consisting of a piezoelectric disc glued on a membrane..... | 29 |
| 2-5 Cross-sectional view of single chamber metal (brass) pump..... | 31 |
| 2-6 Flow rectification in a valveless micropump..... | 32 |
| 2-7 Schematic of (a) conical (b) pyramidal diffuser inlet..... | 33 |
| 2-8 Schematic of a gradually expanding nozzle..... | 34 |
| 2-9 Plot of variation of pressure loss coefficient in a conical diffuser with half angle of the cone for Re= 200, 500,1000 and >30,000..... | 37 |
| 2-10 The computation domain of micropump..... | 38 |
| 2-11 Schematic of the peristaltic pump | 40 |
| 2-12 Representation of pumping cell..... | 41 |
| 3-1 Schematic of the proposed micropump..... | 52 |
| 3-2 Schematic of peristaltic micropump..... | 54 |

| | | |
|------|--|----|
| 4-1 | Design of nozzle/diffuser micropump for NPWT..... | 56 |
| 4-2 | Fixed boundaries at the edges of the diaphragm, brass disc and Piezo disc..... | 61 |
| 4-3 | Symmetry/Work plane of the micropump..... | 62 |
| 4-4 | (a) Formation of mesh (b) Quad Mesh (c) Swept Mesh..... | 64 |
| 4-5 | Deformation of the piezoelectric actuator with applied voltage..... | 65 |
| 4-6 | Displacement of the diaphragm with applied voltage..... | 65 |
| 4-7 | Net fluid flow through the inlet and outlet over time..... | 66 |
| 4-8 | Flow Rates and Volume Conservation..... | 67 |
| 4-9 | (a) Fluid streamline during inflow at time $t = 0.05\text{s}$ (b) outflow at $t = 0.075\text{s}$ | 68 |
| 4-10 | von-Mises stress after piezoelectric actuation at time $t = 0.05\text{s}$ | 68 |
| 4-11 | Velocity field of micropump at time (a) $t=0.05\text{s}$, (b) $t=0.075\text{s}$ | 69 |
| 4-12 | Fluid Velocity Magnitude during inflow..... | 69 |
| 4-13 | Liquid Pressure at $t = 0.05\text{s}$ | 70 |
| 4-14 | Comparison of (a) Inlet and (b) Outlet velocities of different fluid..... | 70 |
| 4-15 | Accumulated flow volume with diffuser length 0.9mm..... | 71 |
| 4-16 | Flow Velocity from Inlet/Outlet for diffuser length 0.9mm..... | 71 |
| 4-17 | Accumulated flow volume with diffuser length 1.1mm..... | 72 |
| 4-18 | Flow Velocity from Inlet/Outlet for diffuser length 1.1mm..... | 72 |
| 4-19 | Accumulated flow volume with diffuser length 1.3mm..... | 73 |
| 4-20 | Flow Velocity from Inlet/Outlet for diffuser length 1.3mm..... | 73 |
| 4-21 | Accumulated flow volume with diffuser length 1.5mm..... | 74 |

| | | |
|------|---|----|
| 4-22 | Flow Velocity from Inlet/Outlet for diffuser length 1.5mm..... | 74 |
| 4-23 | (a) Accumulated flow volume (b) Flow Velocity from Inlet/Outlet for diffuser angle 8° | 75 |
| 4-24 | (a) Accumulated flow volume (b) Flow Velocity from Inlet/Outlet for diffuser angle 9° | 76 |
| 4-25 | (a) Accumulated flow volume (b) Flow Velocity from Inlet/Outlet for diffuser angle 10°..... | 77 |
| 4-26 | Design of the Peristaltic Micropump..... | 78 |
| 4-27 | Principle of Operation of Peristaltic Micropump..... | 78 |

CHAPTER 1

1. INTRODUCTION

Miniaturized pumping devices fabricated by micromachining/macro fabrication techniques are called as micropumps. Micropump is one of the primary components in microfluidic systems. Microfluidic devices are invariably necessary to transport a small amount of fluid from one region to another. Micropumps are essential components of the miniaturization of fluidic systems to enable liquid injection to systems and to control fluidic flow in a variety of applications such as integrated fluidic channel arrangements for chemical analysis systems or electronics cooling as well as for drug delivery systems. Microfluidic systems have numerous advantages like rapid responses, compact size, low-cost, high precision, the potential for mass fabrication, disposability, and portability compared to conventional macro-scale systems (Hsu et al. 2008). Miniaturized pump systems for chemical and biomedical applications have been widely studied. Various types of micropumps have been fabricated on different substrates such as peristaltic micropumps, metallic micropumps, plastic micropumps, as well as valveless piezoelectric micropumps. Among these types, valveless piezoelectric actuated micropumps have the advantage of moderate pressure and displacement at low power consumption, good reliability, and energy efficiency. They also respond rapidly and are widely used due to their ability to conduct particles without support from interior moving mechanical parts, thereby reducing the risk of clogging. A number of different valveless micropumps employing nozzle-diffuser elements have been discussed in the literature. These include piezoelectrically actuated, electromagnetically actuated [1] and bubble micropumps [2]. Use of nozzle-diffuser elements in magneto-hydrodynamic micropumps has also been reported. These pumps utilize the different pressure drop characteristics of flow through a nozzle and a diffuser to direct the flow in one preferential direction, and hence cause a net pumping action. Additional benefits of nozzle-diffuser elements include the ease of manufacture using conventional silicon micromachining techniques, and the much higher flow rates achievable with vibrating diaphragm pumps employing such valves. The higher flow rates, in spite of the poorer flow rectification properties of such valves, stem from the possibility of using valveless micropumps at much higher frequencies as compared to micropumps with passive check valves.

Micro-fluidic system consists of micropump, microsensor, reservoir, and necessary related circuits. Among the microfluidic components, the micropump plays an important role because pumping is the key element of the microfluidic system.

Micropumps are widely used in the field of medical, biomedical applications such as injection of glucose for diabetes patients, insulin injection, blood transportation, DNA hybridization, drug delivery [3], for chemical and biological analysis, other applications are lab-on-chip, fuel cell, automobile application such as fuel cells [4], cooling application like laptop cooling, high flux electronics cooling [5,6], etc.

Micropumps have been developed over the years. Different micropumps are presented during recent years based on different working principles, actuation methods, valve type, chamber combination like serial and parallel, which have their advantages and disadvantages [7]. The micropumps need to fulfill some specific requirements such as low power consumption for actuation, fast response, maximum flow rate, flow control, lightweight, etc. High volumetric flow rate, high resolution, low power consumption, reliability, bio-comparability are the essential requirements of the micropumps [8].

Micropumps are categorized into two types- mechanical and non-mechanical micropumps. Non-mechanical micropump does not involve any mechanical moving parts. Non-mechanical micropumps employ the properties of working fluid to generate the flow. Mechanical type micropumps have moving parts like check valves, membranes, or turbines for delivering a constant fluid flow in every cycle. Shoji et al. categorized the mechanical type micropump actuators into two types, i.e., external actuated micropump and integrated type actuators [9]. The most extensively used micropump is reciprocating/mechanical type micropump, which consists of moving parts like diaphragm and valves. The reciprocating type of micropump works on the principle of deflection of the diaphragm, which is in direct contact with working fluid. The mechanical type of micropumps requires mechanical actuators, which converts one form of energy into another form. The external actuator used in mechanical micropumps is piezoelectric actuator micropump, shape memory type actuator, pneumatic actuator, etc.

Some of the integrated actuators used in micropumps are thermo pneumatic actuators, electrostatic actuators, electromagnetic actuators, etc. There are two methods which can improve

the pumping performance of mechanical type micropumps, one by magnifying the displacement, and the other is to increase the driving voltage.

1.1 Motivation

Now a day's MEMS technologies have been widely used in the microfluidic systems. Microfluidic system performance mainly depends on the efficiency of micropump. Different types of micropumps are designed based on their applications. Micropumps are widely used in the biomedical field such as blood transportation, insulin delivery to control the diabetic's blood sugar level, molecular separation such as DNA analysis, synthesis of nucleic acids for sequencing or synthesis, automotive industries for fuel injection, in chemical and biological sensing. Micropumps are used as electronic cooling systems like lab on chip, micro integrated circuits. Micropumps are used in automobiles for fuel injection.

In this project we will be focusing on two different aspects of application of micropump. The first application of the micropump will focus of wound therapy or which is usually known as the Negative Pressure Wound Therapy (NPWT). The next application will be on the treatment of glaucoma or lowering down the Intraocular Pressure (IOP).

1.2 Wound Therapy

1.2.1 Functional principle of NPWT

The principle of NPWT involves extending the usually narrowly defined suction effect of drainage across the entire area of the wound cavity or surface using open-pore filler that has been fitted to the contours of the wound. To prevent air from being sucked in from the external environment, the wound and the filler that rests inside or upon the wound are hermetically sealed with an airtight adhesive polyurethane drape that is permeable to water vapour, transparent, and bacteria proof. A connection pad is then applied over a small hole that has been made in the drape and connected to a vacuum source by means of a tube (Fig 1).

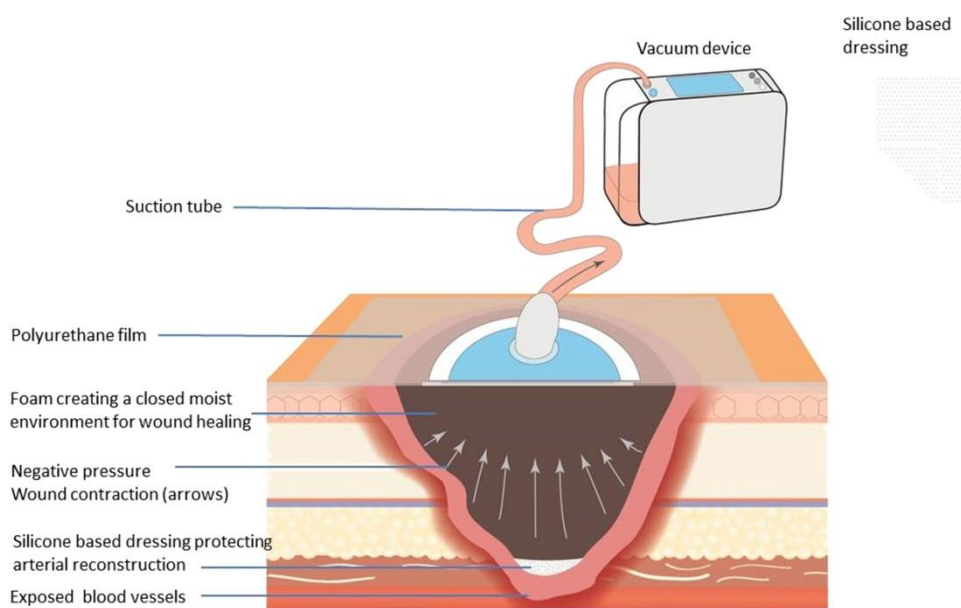


Fig 1-1 – Principle of Negative Pressure Wound Therapy[22]

1.2.2 Mechanism of action of NPWT

The following effects on wound healing and the affected tissue, resulting from applied suction that acts evenly on the entire wound surface, are considered to be the primary clinically significant benefits of NPWT.

Effect on the wound

- Reduction of the wound area due to negative pressure acting on the foam pulls together the edges of the wound (wound retraction).
- Stimulation of granulation tissue formation in an optimally moist wound environment; in several situations even over bradytrophic tissue such as tendons and bone NPWT was able to stimulate granulation tissue formation.
- Continuation of effective mechanical wound cleansing (removal of small tissue debris by suction).
- Effective biochemical reduction of the fluid concentration of wound healing-impairing proteases (such as elastase)—in the first days.
- Reliable, continuous removal of wound exudate (and, consequently, fewer dressing changes) within a closed system.
- Pressure-related reduction of interstitial oedema with consecutive improvement of microcirculation, stimulation of blood flow and oxygenation.

Handling

- Hygienic wound closure—bacteria proof wound dressing for sealing the wound so no external bacteria can enter the wound and the patient's own wound bacteria are not spread. This is particularly important in the event of contamination with problematic bacteria, as in patients with Meticillin-Resistant Staphylococcus Aureus (MRSA)-infected wounds. Thus, it also reduces the risk of cross-infections and development of resistance within the hospital
- Transparent dressing permits continuous clinical monitoring of the surrounding skin through the film with which the wound has been sealed.
- Odourless and hygienic dressing technique; constant seeping through the dressing onto the patient's clothing and bedding can be avoided, reducing demands on the nursing staff.
- Reduction in the number of required dressing changes (only necessary every two to three days), which reduces nursing time requirements, particularly in patients with exuding wounds.

1.2.3 Treatment and the scientific background

NPWT on open wounds NPWT acts in different ways to promote wound healing. The wound is subject to suction pressure that is propagated through the wound filler to the wound bed. This suction drains exudate from the wound and creates a mechanical force in the wound edges that result in an altered tissue perfusion, angiogenesis and the formation of granulation tissue. Some of the mechanisms of action have been demonstrated experimentally and clinically. The effects can be summarized as follows:

- Isolating the wound from infection of external origin
- Creating a moist wound environment
- Pressure transmission and removal of exudate
- Removal of oedema
- Mechanical stress of the wound edges
- Altered blood perfusion
- Angiogenesis and the formation of granulation tissue.

NPWT isolates the wound and prevents it from being infected by the external environment. NPWT also involves sealing the wound with an airtight drape that will create a moist wound environment.

Creating a moist wound environment and removal of exudate

A moist environment is vital in wound healing as it facilitates the re-epithelialisation process. However, in an overly moist wound, exudate may cause infection and maceration, leading to damage to the wound edge. Removal of exudate is important to prevent the accumulation of necrotic tissue and slough that tend to continually accumulate in wounds and alter the biochemical and cellular environment. Stagnant wound fluid may also increase the risk of abscesses. The accumulation of necrotic tissue or slough in a wound promotes bacterial

colonisation and hinders repair of the wound. NPWT balances these effects, providing a moist wound environment while removing excess fluid. [10,11,12]

Removal of oedema

Oedema causes increased pressure on the wound tissue, which in turn compromises the microvascular blood flow, reducing the inflow of nutrients and oxygen. This reduces resistance to infections and inhibits healing, thus, in order to facilitate wound healing, it is important to reduce tissue oedema. NPWT causes compression of the tissue closest to the surface of the wound, which is believed to reduce interstitial oedema [13, 14]. There are few studies but there is widespread agreement among clinicians that NPWT eliminates tissue oedema. However, there are only a handful studies that have directly measured this effect [11, 12, 15], NPWT resulted in increased perfusion in patients with bilateral hand burns and it was concluded that oedema was reduced. In an experimental study on the pig septic open abdomen, it was shown that the NPWT-treated pigs had less tissue oedema than those treated by passive drainage.[16] High-frequency ultrasound has been used to quantify reduction of oedema in the periwound tissue in a small group of pressure ulcer (PU) patients on commencement of NPWT.[17] Most probably, oedema and exudate are reduced both directly through mechanical removal of excess fluid, and indirectly through altered microcirculation.

Mechanical effects on wound edges

NPWT mechanically stimulates the wound bed, and produces a suction pressure on the wound edges that will push onto the wound and contract it [10, 11, 12]. The mechanical effects lead to tissue remodeling that may facilitate wound closure. It also has been found that the wound tissue and the filler material interact on a microscopic level to micro deform the tissue. These mechanical deformations lead to a number of biochemical reactions and gene transcriptions. The wound bed is drawn into the pores of the foam or in-between the threads of the gauze. These mechanical effects affect the cytoskeleton of the cells and initiate a cascade of biological reactions that may accelerate the formation of granulation tissue and subsequent wound healing. The mechanotransductive stimulus on the wound bed that is exerted by the foam under suction is regarded as an important effect of NPWT [10]. Mechanical tissue deformation stimulates the expression of the angiogenic growth factors and receptors such as vascular endothelial growth

factor (VEGF). Previous In-vitro studies have shown stretching of endothelial cells stimulates the blood vessel formation.

Change in bacterial count, bacterial clearance and immunological effects

NPWT offers a closed system for wound healing, as the adhesive drape provides a barrier against secondary infection from an external source and has been suggested to reduce the bacterial load in the wound. A reduction of the wound infection rate and the degree of bacterial load has been described as a secondary endpoint in several publications. [18,19]

Molecular mechanisms in wound healing

The positive effects of NPWT are attributed to the effects of the vacuum-related mechanical stimulus on cell function, protein synthesis and gene expression with resulting matrix-molecule synthesis and cell proliferation. [10, 20] However, this explanation is given as a mere conclusion by analogy to the results of the scientific investigation of the effects of callus distraction. In fact, there are hardly any studies that investigate the cellular effects of NPWT.

Pressure level/suction strength

There is an accumulation of evidence suggesting the effective range of negative pressure is between -50 mmHg and -150 mm Hg. [21] There is however, little information on the optimum level of negative pressure for clinical use and it has been speculated that the level of negative pressure may be adjusted in a number of circumstances. Pressure distribution into the wound depends on the direct contact between the wound filler and the wound tissues. Tissue that is not in contact with the wound filler will not be subject to suction force, as seen in a sternotomy study. A wound contact layer slightly lowers the level of negative pressure that affects the tissue level.

Morphology of Wounds

There are different types and shapes of wounds as shown in Fig 1-2. Wounds may be uniform or have irregular beds with or without the presence of undermining. Foam may fit better into a wound with a uniform shape, while gauze may be easier to apply in wounds that have an irregular shape, or with undermining since it can be better manipulated to the shape of the

wounds. Different wound fillers can also be combined. In deep wounds, with or without association with an area that is undermined, both fillers may be applied in order to fill the wound efficiently. Over a thin graft or a wound sleeve, the gauze also allows us to cover the entire wound in an appropriate manner. Negative pressure is only transmitted to the tissues that are in immediate contact with the wound filler. In complicated wounds with deep pockets, the wound filler must be carefully positioned, and it may be easier to use gauze because it can be adapted to the shape of the wound. Foam may be advantageous for ‘bridging therapy’ since the foam compresses to a greater extent than, for example, gauze and thereby contracts the wound and speeds up the closure.



FIG 1-2- *Different types of Wound for NPWT*

Exuding wounds: In heavily exuding wounds, a higher pressure (-120mmHg) may be useful, since foam is less dense than gauze and a higher level of negative pressure drains the wound quicker.

1.3 Intraocular Pressure (IOP) / Glaucoma

The eye includes a cornea and crystalline lens that form an image on the retina of the eye. The retina of the eye senses the light image formed thereon and transmits neural signals via the optic nerve to the occipital cortex of the brain, Such that the person can see and perceive his or her Surroundings. Unfortunately, ocular diseases can compromise vision of the eye and may cause blindness in at least some instances. Glaucoma is a major cause of blindness in the United States. In many instances, glaucoma related blindness can be prevented if caught and managed early. Glaucoma is usually associated with an increase in intraocular pressure (hereinafter "IOP), that can result in damage to the retina of the eye. Because glaucoma is usually associated with an increase in IOP periodic testing can be used to monitor glaucoma in order to prevent irreversible vision loss. For example, a person may undergo two to four exams per year in an ophthalmologist's office, although more examination may sometimes occur. Although treatment can be effective in many instances, in at least some patients may continue to lose vision under physician directed care. For example, about fifteen percent of patients under fifty years of age may continue to lose vision when receiving care and about thirty percent of patient over sixty may continue to lose vision.

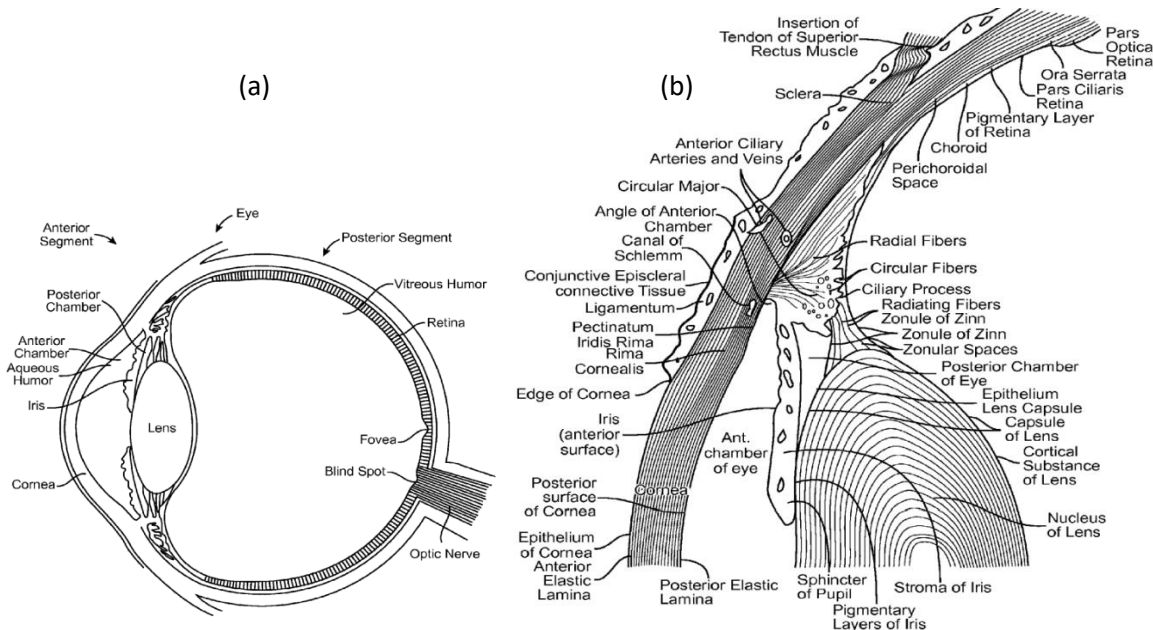


Fig 1-3-(a) Structure of the Human Eye (b) Distinct description of the eye from where aqueous humor flows [24]

A significant clinical need exists to detect elevated IOP such that appropriate medical and surgical treatment can be delivered to control the patient's IOP and pump out the fluid to decrease vision loss. Unfortunately, at least some of the current clinical techniques for measuring glaucoma may not detect elevated IOP, Such that a patient can lose vision and may even become blind in at least some instances. For example, an ophthalmic exam may only measure IOP when the patient is in the eye clinic. In at least some instances, the patient may undergo an increase in IOP for example a pressure spike, when the patient is away from the clinic. As such pressure spikes may not be detected; the patient may not receive treatment in time to mitigate vision loss. Further, at least some patients may not be able to visit the eye clinic on a strict regular basis, for example elderly patients and children, such that an increase in IOP may not be detected in a timely manner so as to prevent vision loss in at least some instances. Also, in at least some instances a patient may simply forget to take his or her medicine. Such that the patient fails to follow the prescribed treatment.

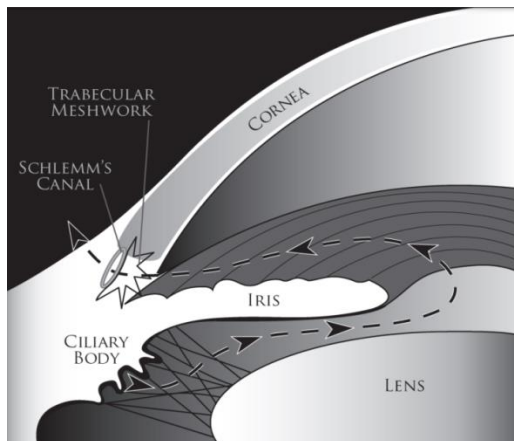


Fig 1-4 – Schematic diagram illustrating the trabecular meshwork conventional outflow pathway.

Aqueous humor is produced by the ciliary body and it flows (dashed line shown with arrowheads) from the posterior chamber through the pupil into the anterior chamber. From there it flows out through the trabecular meshwork into the Schlemm's canal and subsequently absorbed into the episcleral veins via the collector channels.[23]

Glaucoma damages the optic nerve which carries visual signal information from the eye to the brain. Patients with glaucoma initially lose their peripheral vision. If left untreated, the patients lose their vision completely. Glaucoma affects an estimated 67 million people worldwide; including over 3 million Americans aged 40 years and older [25]. Approximately 120,000 are

blind from glaucoma; accounting for 9%-12% of all cases of blindness in the U.S. Glaucoma is the second leading cause of blindness in the U.S. and the first leading cause of irreversible blindness.

The most common type of glaucoma is open-angle glaucoma and it accounts for about 90% of all glaucoma diagnosed cases [4]. In patients with open-angle glaucoma, the angle in the eye where the iris meets the cornea is open but the Schlemm's canal and trabecular meshwork become clogged overtime leading to a mismatch between the inflow and outflow of intraocular fluid. Open-angle glaucoma develops over a period of time without any noticeable symptoms. Since the visual acuity remains intact until late in the disease, it is harder for the patient to notice any change in the quality of the vision during initial periods of disease progression. Unlike open-angle glaucoma, angle-closure glaucoma develops suddenly due to blocked drainage canals. Blocked drainage canals are a result of bunching up of outer edges of iris over the canal surface. This leads to a sudden spike in IOP.

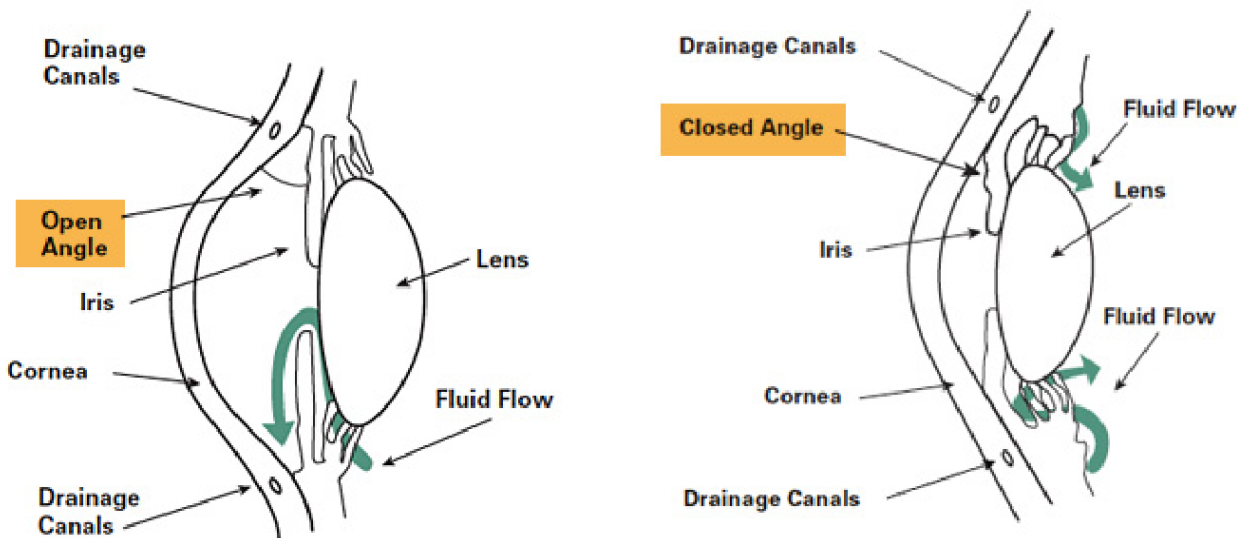


FIG 1-5- Open-angle and angle-closure glaucoma [26]

Compared to open-angle glaucoma, angle-closure glaucoma is rare and the treatment is relatively simple. Figure 1-5 shows the IOP fluid flow paths for both open-angle and angle-closure glaucoma. Other variants of glaucoma include low-tension glaucoma, congenital glaucoma, and

secondary glaucoma caused by diseases such as diabetes. Normal IOP is in the range of 10-21 mmHg [27, 28] but in glaucoma patients, IOP increases above the normal range because of increased resistance to the fluid flow in the drainage pathway. Elevated IOP is associated with loss of optic nerve tissue, loss of peripheral vision, and leads to blindness if not treated. IOP measurement, optic disc examination, and visual field testing are used for glaucoma diagnosis. Regular monitoring of the above three parameters is important for disease management. Early treatment helps to slow disease progression. However, early signs are detectable only by a physician. This is especially true in open angle glaucoma, which is typically symptom-free in the early stages. Current treatment is directed towards reducing the IOP, which has been shown to decrease disease progression. Medications in the form of eye drops are commonly used to lower IOP. These help either by decreasing the aqueous fluid production or by reducing the resistance to aqueous outflow via trabecular meshwork and uveoscleral route [23].

1.3.1 Standard Techniques for IOP Measurement

The standard way of measuring the IOP is by determining the resistance of the cornea to indentation using an instrument called tonometer. There are several indentation techniques in practice. Some of them are discussed below.

1.3.1.1 Applanation (Goldmann) Tonometry

Goldmann Applanation Tonometer (GAT) is considered as “gold standard” for measuring IOP [29]. It is based on Imbert-Flick principle, which states that the pressure inside the liquid filled sphere can be determined by the force required to flatten a portion of the sphere. GAT uses a probe to flatten a portion of the cornea and a slit lamp microscope is used to examine the eye. The pressure within the eye is calibrated to the weight required to flatten 3.06 mm² of the cornea. This is the minimal area of applanation needed to give accurate results, yet, causing only an increase of 2.5% in IOP. Even though the GAT measurements are accurate to within 0.5 mmHg for IOPs of 20 mmHg or lower, they are dependent on corneal thickness. A thinner cornea than normal would appenate more thereby providing underestimation of the pressure. Similarly, a thicker cornea than normal would overestimate the IOP [32–34]. Corneal rigidity

and central corneal thickness differs between patients. Several correction factors are needed to get accurate measurements.

1.3.1.2 Non-contact Tonometry (Pneumotonometry)

In non-contact tonometry, instead of a probe, an air jet is directed at the cornea to flatten a portion of it. Captured light reflected from the flat portion of the cornea gets used to determine the size of the flattened area. Once a predetermined flattening diameter is achieved, the corresponding pressure is used to estimate the IOP. This method does not require the cornea surface to be anesthetized and hence can be used to make large number of measurements. Over the years, various portable tonometers have been developed. However, it is not possible to measure the IOP continuously by using these techniques.

1.3.2 Need for Continuous IOP Measurement

Patients with glaucoma can be mistakenly considered to be “well controlled” if their mean IOP is lower than 21 mm Hg. However, a well-known fact is that many glaucoma patients continue to progressively lose visual field, despite having IOPs that are considered “well controlled.” One possible explanation could be that progression is due to IOP variations within the acceptable limit. Asrani et al. [25], after monitoring 105 human eyes with homeuse tonometry, reported that in glaucoma patients with office IOP in the “normal” range, large fluctuations in diurnal IOP were a significant risk factor, independent of parameters obtained in the office. Several clinical studies [26–32] found that 24 hour monitoring may reveal IOP fluctuations that may help in better design of treatment methodologies. Treatment of glaucoma involves knowing that the pharmacologic treatment is effective and the pressure fluctuation does not exceed the allowable limits. Multiple or continuous measurement of the IOP in glaucoma patients may help in better disease diagnosis, monitoring, and management. Frequent/continuous data collection (IOP measurements) may impact glaucoma treatment similar to the impact of home glucose monitoring on the management of diabetes.

1.4 Thesis Outline

Here, Chapter 1 we have discussed about the ongoing problems and research related to biomedical domains especially in wound therapy and the treatment of Glaucoma. It serves the main motivation towards this project which deals with application of MEMS micropumps to treat severe wounds not only outside but also for in-vitro applications and also for the treatment of glaucoma, to pump out the excess fluid to lower down the Intraocular Pressure.

In Chapter 2, we will discuss about the early research works on MEMS micropumps and also their actuation mechanism. We will see how to model pumps so that design of such pumps complies with the theoretical considerations.

In Chapter 3, we will discuss about how to apply these micropumps for the treatment of the diseases. We will describe in detail the possibilities of future work.

In Chapter 4, we will design, simulate and develop such micropumps for the implementation. We will compare geometries to obtain the optimal figure and discuss the results.

References

- [1] Hintermüller, M.A.; Jakoby, B. A Diffusor/Nozzle Pump Based on a Magnetically Actuated Flexible PCB Diaphragm. *Proceedings* **2018**, *2*, 1077.
- [2] Jr-Hung Tsai and Liwei Lin, "A thermal-bubble-actuated micronozzle-diffuser pump," in Journal of Microelectromechanical Systems, vol. 11, no. 6, pp. 665-671, Dec. 2002, doi: 10.1109/JMEMS.2002.802909.
- [3] A. Nisar, Nitin Afzulpurkar, Banchong Mahaisavariya, Adisorn Tuantranont, MEMS-based micropumps in drug delivery and biomedical applications, Sensors and Actuators B: Chemical, Volume 130, Issue 2, 2008, Pages 917-942, ISSN 0925-4005.
- [4] Tao Zhang, Qing-Ming Wang, Valveless piezoelectric micropump for fuel delivery in direct methanol fuel cell (DMFC) devices, Journal of Power Sources, Volume 140, Issue 1, 2005, Pages 72-80.
- [5] Laser D J et al 2003 Silicon electroosmotic micropumps for IC thermal management Proc. Transducers '03 (Boston, MA)
- [6] Dau, Van & Dinh, Thien & Sugiyama, Susumu. (2009). A MEMS-based silicon micropump with intersecting channels and integrated hotwires. *Journal of Micromechanics and Microengineering*. **19**. 125016. 10.1088/0960-1317/19/12/125016.
- [7] Nguyen N, Huang X, Chuan TK (2002). MEMS-Micropumps: A Review. *Journal of Fluids Engineering* **124**: 384–392.
- [8] N.C. Tsai, C.Y. Sue, Review of MEMS-based drug delivery and dosing systems. *Sens Actuators A Phys* **134**(2), 555–564 (2007)
- [9] Shoji, Shuchi and Masayoshi Esashi. "Microflow devices and systems." *Journal of Micromechanics and Microengineering* **4** (1994): 157-171.
- [10] Morykwas, M.J., Argenta, L.C., Shelton-Brown, E.I., McGuirt, W. Vacuumassisted closure: a new method for wound control and treatment: animal studies and basic foundation. *Ann Plast Surg* **1997**; *38*: 6, 553–562
- [11] Argenta, L.C., Morykwas, M.J. Vacuum-assisted closure: a new method for wound control and treatment: clinical experience. *Ann Plast Surg* **1997**; *38*: 6, 563–577.

- [12] Morykwas. M.J., Simpson. J., Punger, K. et al. Vacuum-assisted closure: state of basic research and physiologic foundation. *Plast Reconstr Surg* 2006; 11: 7 Supplement, 121S–126S.
- [13] Kairinos, N., Solomons, M., Hudson, D.A. Negative-pressure wound therapy I: the paradox of negative-pressure wound therapy. *Plast Reconstr Surg* 2009; 123: 2, 589–600.
- [14] Kairinos, N., Solomons, M., Hudson, D.A. The paradox of negative pressure wound therapy – in vitro studies. *J Plast Reconstr Aesthet Surg* 2010; 63: 174-179
- [15] Webb, L.X. New techniques in wound management: vacuum-assisted wound closure. *J Am Acad Orthop Surg* 2002; 10: 5, 303–311.
- [16] Kubiak, B.D., Albert, S.P., Gatto, L.A. et al. Peritoneal negative pressure therapy prevents multiple organ injury in a chronic porcine sepsis and ischemia/reperfusion model. *Shock* 2010; 34: 5, 525–534.
- [17] Young, S.R., Hampton, S., Martin, R. Non-invasive assessment of negative pressure wound therapy using high frequency diagnostic ultrasound: oedema reduction and new tissue accumulation. *Int Wound J* 2013; 10: 4, 383–388.
- [18] Deva, A.K., Buckland, G.H., Fisher, E. et al. Topical negative pressure in wound management. *Med J Aust* 2000; 173: 3, 128–131.
- [19] Fleck, T.M., Fleck, M., Moidl, R. et al. The vacuum-assisted closure system for the treatment of deep sternal wound infections after cardiac surgery. *Ann Thorac Surg* 2002; 74: 5, 1596–1600
- [20] Mouës, C.M., Vos, M.C., Van Den Bemd, G.J. et al. Bacterial load in relation to vacuum-assisted closure wound therapy: A prospective randomized trial. *Wound Repair Regen* 2004; 12: 1, 11–17.
- [21] Birke-Sorensen, H., Malmsjö, M., Rome, P. et al. Evidence-based recommendations for negative pressure wound therapy: treatment variables (pressure levels, wound filler and contact layer) – Steps towards an international consensus. *J Plast Reconstr Aesthet Surg* 2011; 64: Suppl, S1–S16.
- [22] Andersson S, Monsen C, Acosta S. Outcome and Complications Using Negative Pressure Wound Therapy in the Groin for Perivasculär Surgical Site Infections after Vascular Surgery. *Ann Vasc Surg*. 2018 Apr;48:104-110. doi: 10.1016/j.avsg.2017.10.018. Epub 2017 Dec 5. PMID: 29217444.
- [23] Goel M, Picciani RG, Lee RK, Bhattacharya SK. Aqueous humor dynamics: a review. *Open Ophthalmol J*. 2010;4:52-59. Published 2010 Sep 3.

- [24] National Center for Biotechnology Information (2022). PubChem Patent Summary for CN-102711593-A. Retrieved June 16, 2022 from <https://pubchem.ncbi.nlm.nih.gov/patent/CN-102711593-A>.
- [25] H. Quigley. Number of people with glaucoma worldwide. *British Journal of Ophthalmology*, 80:389–393, 1996
- [26] <http://www.glaucoma.org/glaucoma/>.
- [27] L. Titcomb. Treatment of glaucoma: Part 1. *Pharmaceutical J.*, 263:324–329
- [28] J.M. Tielsch, J. Katz, K. Singh, H. Quigley, J.D. Gottsch, J. Javitt, and A. Sommer. A population-based evaluation of glaucoma screening: The baltimore eye survey. *American Journal of Epidemiology*, 134:1102–1110, 1991
- [29] R. A. Moses. The goldmann applanation tonometer. *American Journal of Ophthalmology*, 46:865–869, 1958.
- [30] J. Gloster and E.S. Perkins. The validity of the imbert-flick law as applied to applanation tonometry. *Exp. Eye Res.*, 44:274–283, 1963.
- [31] N. Ehlers, T. Bramsen, and S. Sperling. Applanation tonometry and central corneal thickness. *Acta Ophthalmol*, 53:34, 1975.
- [32] J.D. Brandt, J. Beiser, and M.A. Kass. Central corneal thickness in the ocular hypertension treatment study (ohsts) ophthalmology. *Ophthalmology*, 108:1779–1778, 2001.
- [33] P.J. Foster, J. Baasanhu, P.H. Alsbrik, D. Munkhbayar, and G.J. Johnson. Central corneal thickness and intraocular pressure in a mongolian population. *Ophthalmology*, 105:969–973, 1998
- [34] L.J. Phillips, C.J. Cakanac, M.W. Eger, and Lilly. Central corneal thickness and measured iop: A clinical study. *Optometry*, 74:218–225, 2003.

CHAPTER 2

Literature Review and Theoretical Analysis

2. MEMS Micropumps

Micropumps are essential components of the miniaturization of fluidic systems to enable liquid injection to systems and to control fluidic flow in a variety of applications such as integrated fluidic channel arrangements for chemical analysis systems or electronics cooling as well as for drug delivery systems. Micropumps offer important advantages because they are compact and small in size, they can operate using small sample volumes, and they provide rapid respond time. Miniaturized pump systems for chemical and biomedical applications have been widely studied. Research on micropumps was initiated in 1980 and numerous different pumps have since been developed [1]. They can be manufactured in different materials, but mostly silicon and glass have been used as bulk materials. During the last years plastic has been shown to be a competitive alternative. Different pump principles are conceivable. They can generally be classified into two groups: mechanical and non-mechanical (without moving parts) [2]. At least three kinds of mechanical micropumps have been developed: peristaltic [3], reciprocating [4-6] and rotary [7] pumps.

2.1 Actuation Principles

Today actuators are an important part of MST. Consequently a lot of research is devoted to actuators. Actuators are needed to transfer input energy, e.g. electric or thermal energy, into work output, e.g. motion, heat or light (see Fig. 2-1). Many resonant sensors, e.g. gyros, require actuators to drive them. Actuators can be used to build in self-testing in sensors that previously only had detection capabilities. Microsystems that require mechanical output need actuators. Examples of such systems are micromirrors used to scan laser beams or to switch them from one fiber to another. In microfluidic system and microanalysis systems actuators are needed for pumps and valves. They can also be used for switches, relays, etc., in microelectromechanical devices for wireless communications.

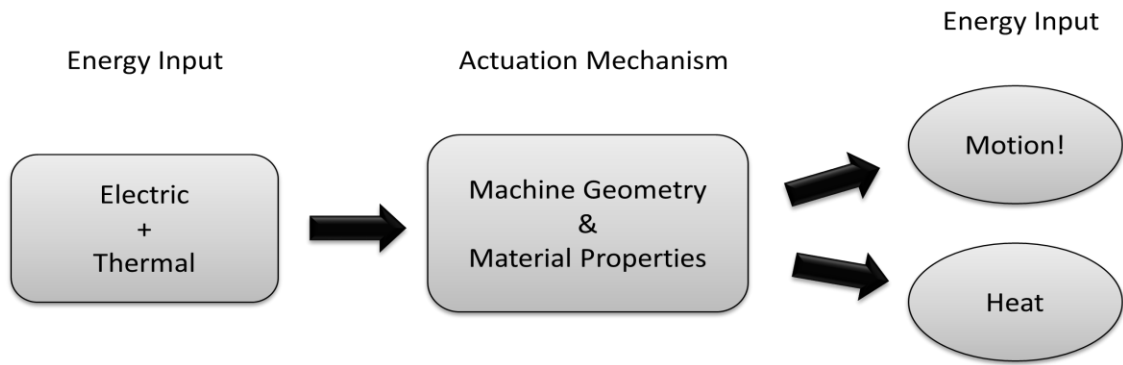


FIG 2-1 - A schematic figure of the transfer of input energy to output work in an actuator

Many different solutions for actuation of micromechanical devices have been proposed. Piezoelectric actuation is probably the most commonly used method for micropumps but other methods have also been used, e.g. electrostatic, pneumatic and thermo-pneumatic excitation. During this project the focus was on the pump principle rather than the actuation principle. Piezoelectric actuation was chosen because it can easily be applied to the individual pumps after the micromachining process.

2.1.1 Piezoelectric Sensing and Actuation

The piezoelectric effect has been widely used for micromechanical devices. The effect was discovered by Jacques and Pierre Curie in 1880. They discovered that if special crystals were subject to mechanical tension, they became electrically polarized and the polarization was proportional to the extension. They also discovered that the opposite was true; if an electrical field was applied across the material it deformed. This is known as the inverse piezoelectric effect.

The piezoelectricity phenomena was developed and applied in sonar and quartz oscillation crystals. In 1921, Walter Cady invented the quartz crystal-controlled oscillator and the narrow-band quartz crystal filter used in communication systems. The World War II spurred the growth of this field, especially with the urgent needs by the military to detect submarines. Two important artificial piezoelectric crystals, barium titanate and lead zirconate titanate were invented in the early 1950s. These materials are not naturally-occurring piezoelectric materials.

Rather, they are synthesized materials and they must be electrically poled in order to exhibit significant piezoelectric effects. In 1958, synthetic quartz material became available.

Now, piezoelectric materials are being used in MEMS sensors and actuators. Thin film piezoelectric materials has been explored for use as on-chip acoustic transducers [8], pumps and valves for liquid and particles [9, 10], accelerometers [11, 12], speaker and microphones [13, 14], mirrors [15], and chemical sensors [16], among others.

Many important properties of piezoelectric materials stem from its crystalline structures. Piezoelectric crystals can be considered as a mass of minute crystallites (domains). The macroscopic behavior of the crystal differs from that of individual crystallites, due to orientation of such crystallites. The direction of polarization between neighboring crystal domains can differ by or owing to random distribution of domains throughout the material, no overall polarization or piezoelectric effect is exhibited. A crystal can be made piezoelectric in any chosen direction by poling, which involves exposing it to a strong electric field at an elevated temperature. Under the action of this field, domains most nearly aligned with the field will grow at the expense of others. The material will also lengthen in the direction of the field. When the field is removed, the dipoles remain locked in approximate alignment, giving the crystal a remnant polarization and a permanent deformation,

The poling treatment is usually the final step of crystal manufacturing. Care must be taken in all subsequent handling and use to ensure that the crystal is not depolarized, since this will result in partial or even total loss of its piezoelectric effect. A crystal may be depolarized mechanically, electrically, or thermally. Mechanisms for depolarization are further explained in the following. Exposure to a strong electric field of opposite polarity to the poling field will depolarize a piezoelectric element. The field strength required for marked depolarization depends on the material grade, the time the material is subjected to the depolarization field, and the temperature.

Mechanical depolarization occurs when mechanical stress on a piezoelectric element becomes high enough to disturb the orientation of the domains and hence destroy the alignment of the dipoles. The safety limits for mechanical stress vary considerably with material grade. If a piezoelectric element is heated to a certain threshold temperature, the crystal vibration may be so strong that domains become disordered and the element becomes completely depolarized. This

critical temperature is called the Curie point or the Curie temperature. A safe operating temperature would normally be half way between and the Curie point.

2.1.2 Mathematical Description of Piezoelectric Effects

Piezoelectric materials are crystals. The microscopic origin of piezoelectricity is the displacement of ionic charges within a crystal, leading to polarization and hence electric field.

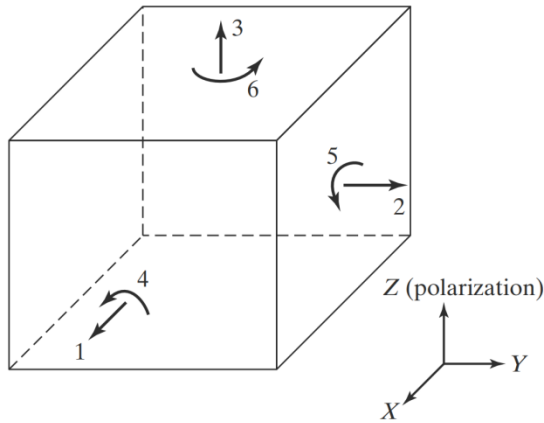


FIG 2-2- Schematic illustration of piezoelectric crystal in a rectangular system. [17]

A stress (tensile or compressive) applied to a piezoelectric crystal will alter the spacing between centers of positive and negative charge sites in each domain cell, leading to a net polarization manifested as open circuit voltages measurable at the crystal surface. Compressive and tensile stresses will generate electric fields and hence voltages of opposite polarity. Inversely, an external electric field will exert a force between the centers of positive and negative charges, leading to an elastic strain and changes of dimensions depending on the field polarity. Not all naturally occurring or synthesized crystals exhibit piezoelectricity. Crystals can be classified into 32 groups according to crystal symmetry. Centrosymmetric crystal structures are crystals that are symmetric along all axes through the center of the crystal. These crystals occupy 11 out of 32 possible groups and are non-piezoelectric materials because the positive and negative charge sites will not be spatially separated under stress. Out of 21 non-centrosymmetric groups, 20 are piezoelectric crystals. Piezoelectric effects are strongly orientation dependent. The notation conventions for crystal orientations in the context of piezoelectric polarization are discussed first. A piezoelectric material needs to be poled in a particular direction to provide a strong

piezoelectric effect, although some materials exhibit natural or spontaneous polarization. The direction of positive polarization is customarily chosen to coincide with the Z-axis of a rectangular system of crystallographic axes X, Y, and Z. Alternatively, the normal stress components along axes X, Y, and Z are denoted by subscripts 1, 2, and 3, respectively. As such, the poling axis always coincides with axis 3. Shear stress and strain components about these axes are denoted by subscripts 4, 5, and 6, respectively. This can be seen in Fig 2-2.

Piezoelectricity involves the interaction between the electrical and mechanical behavior of the medium.

To the first order this is described as-

$$S = s^E T + dE \quad (2-1)$$

Where, S is the strain, s^E is the compliance tensor under conditions of constant electric field, T is the stress, d is the piezoelectric charge constant tensor and E is the electric field. The deformation of a piezoelectric crystal is illustrated in Fig. 2-3.

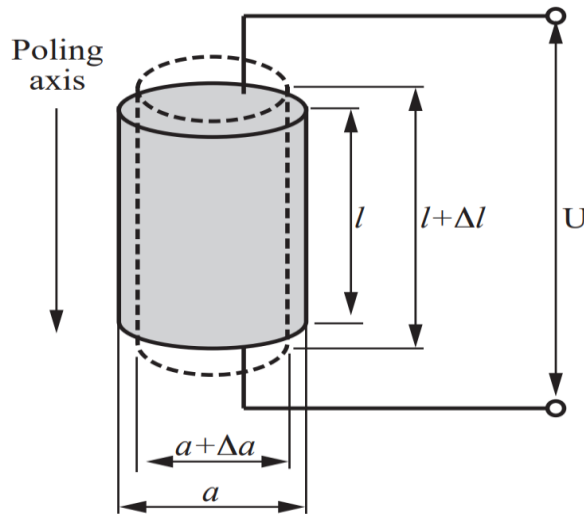


FIG 2-3 - The deformation of a piezoelectric device when subject to an electrical voltage[18]

In the absence of mechanical loads Eq. (2-1) gives-

$$\Delta l = d_{33} \cdot U = d_{33} \cdot \frac{U}{l} \cdot l = d_{33} \cdot E \cdot l \quad (2-2)$$

and,

$$\Delta a = d_{31} \cdot U = d_{31} \cdot \frac{U}{l} \cdot l = d_{31} \cdot E \cdot a \quad (2-3)$$

Where, Δl is elongation along the poling axis, l is the device length along the poling axis, U is the electrical voltage, Δa is elongation perpendicular the poling axis and a is the device length perpendicular to the poling axis. Normally, $d_{33} > 0$ and $d_{31} < 0$.

Examples of piezoelectric materials are quartz, LiTaO₃, PZT and ZnO. Non-piezoelectric materials, e.g. silicon, can be excited by depositing a thin film of a piezoelectric material, e.g. PZT or ZnO. Another solution is to mount a piezoelectric disk on the non-piezoelectric material. This eliminates the problem of making the film thick enough that high voltages can be applied without dielectric breakdown (sparks/short circuits across the film). The piezoelectric effect can be used to bend a diaphragm, e.g., in a pump. The principle is illustrated in Fig. 2-4 where a piezoelectric disk is glued to a diaphragm. When a voltage is applied across the piezoelectric disc it deforms and forces the diaphragm to bend.

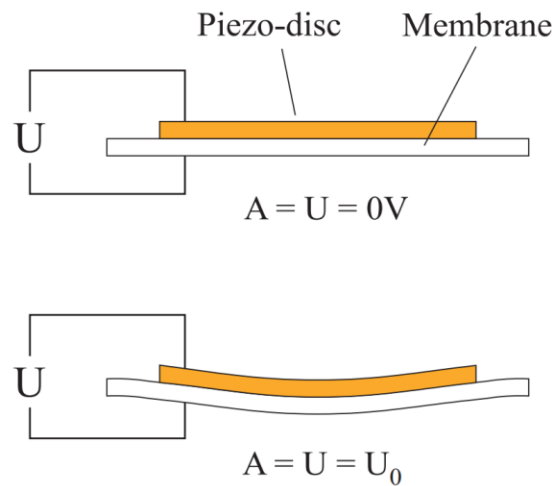


FIG 2-4- *The bending of a bimorph consisting of a piezoelectric disc glued on a membrane. This can be used for diaphragm pumps.*

In literature, several micropumps have been fabricated in accordance with different applications. Merits and De-Merits of such pumps were taken into account for the

In Table 2-1 the performances of some mechanical micropumps are summarized. The pumps that have attracted most attention are reciprocating diaphragm pumps, mainly because of the broad range of fluids which can be pumped and because the pumps are readily realized using silicon micromechanics. In non-mechanical micropumps the electrodynamic effect, electro-osmotic phenomena and ultrasonic effect are used among others [2].

| Author [ref] | year | Pump principle | Actuation mechanism | Pump frequency | Volume flow[μl/min] [Hz] | Pressure head [kPa] | Size [mm] |
|----------------------------|-------------|------------------------------------|--------------------------------|---------------------------|--|--------------------------------|------------------|
| Ahn 1995 [20] | | Jet-type rotary | electromagnetic | 83 | 24 | - | 2x2x0.16 |
| Smits 1990 [21] | | Peristaltic | piezoelectric, disc type | 15 | 100 | 6 | - |
| Mizoguchi 1992 [22] | | " | laser | 3 | 5 | 0.3 | - |
| van Lintel et al 1988 [23] | | Reciprocating, check-valves | piezoelectric, disc type | 3 | 8 | 10 | 50x2 |
| van de Pol et al 1990 [24] | | " | thermopneumatic | 1 | 34 | 5 | 13x45x2 |
| Shoji et al 1990 [25] | | " | piezoelectric, stack type | 40 | 40 | 15 | 20x20x1 |
| Zengerle et al 1992 [26] | | " | electrostatic | 25 | 70 | 2.5 | 7x7x2 |
| Lammerink et al 1993 [27] | | " | thermopneumatic | 5 | 60 | 4 | 13x45x2 |
| Stemme& Stemme 1993 [28] | | Reciprocating, valve-less diffuser | piezoelectric, disc type | 300 | 3000 | 25 | 19x5 |
| Olsson et al 1994 | | " | piezoelectric, disc type | 560 | 16000 | 17 | 36x36x1 |
| Gerlach et al 1994 [29-31] | | Reciprocating, valve-less nozzle | piezoelectric, disc type | 8000 | 480 | 3.3 | - |
| Olsson et al 1995 | | Reciprocating, valve-less diffuser | piezoelectric, disc type | 1300 | 225 | 17 | 15x18x1 |
| Zengerle et al 1995 [32] | | Reciprocating, check-valves | electrostatic | 0-1000 | 350 | 31 | 7x7x2 |
| Zengerle et al 1996 [33] | | Reciprocating, active-valves | piezoelectric | 60 | 1600 | 17 | 7.3x7.3 |
| Olsson et al 1996 | | Reciprocating, valve-less diffuser | piezoelectric, disc type | 3000-4000 | 2300 | 74 | 15x17x1 |
| Kämper et al 1998 [34] | | Reciprocating, check-valves | piezoelectric, disc type | 50-70 | 400 | 210 | 12x12x3.5 |
| Linnemann et al 1998 [35] | | Reciprocating, check-valves | piezoelectric, disc type | 220 | 1400 | 1000 | 7x7x1 |

Among the following variations of the micropumps, two micropumps will be discussed in this project which is applied to the different applications in the bio-medical domain. These two micropumps are- Valveless Diffuser Micropumps and Peristaltic Micropump.

2.2 Valveless Micropumps

Valve-less reciprocating pumps have flow channels at the inlet and the outlet that are designed to have different flow resistances in the forward and the reverse directions. This eliminates wear and fatigue in the check-valves and reduces the risk of valve clogging. The idea to use such channels in pumps was mentioned in 1989 [36] and a finite element analysis of micromachined nozzles used as such channels was presented in 1990 [37].

The first valve-less reciprocating pump was the valve-less diffuser pump presented in 1993 [6, 38] and illustrated in Fig. 2-5. In the diffuser pump diffuser elements are used as the flow directing elements. The opening angles of the diffusers are small, normally less than 20° , and the diffuser direction is the positive flow direction.

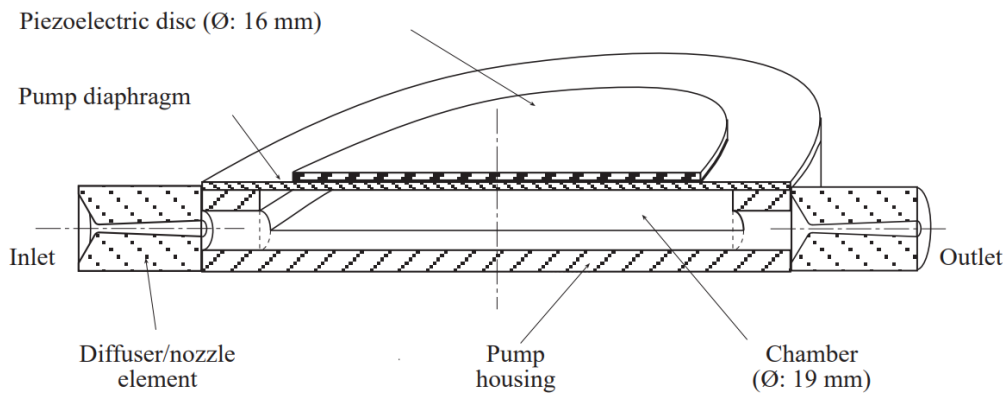


FIG 2-5- Cross-sectional view of the single-chamber metal (brass) pump consisting of a circular housing with an oscillating top diaphragm and two conical diffuser elements[6]

2.2.1 Principle of Operation

The operating principle of a valveless micropump is illustrated in Fig.2-6. The particular flow characteristics shown are for small nozzle-diffuser angles. In the expansion mode, as the volume

of the pumping chamber increases, more fluid enters the pumping chamber from the element on the right which acts like a diffuser (and hence offers less flow resistance) than the element on the left, which acts like a nozzle. On the other hand, in the contraction mode, more fluid goes out of the element on the left which now acts as a diffuser, while the element on the right acts as a nozzle. Hence, net fluid transport is achieved in the pumping chamber from right to left.

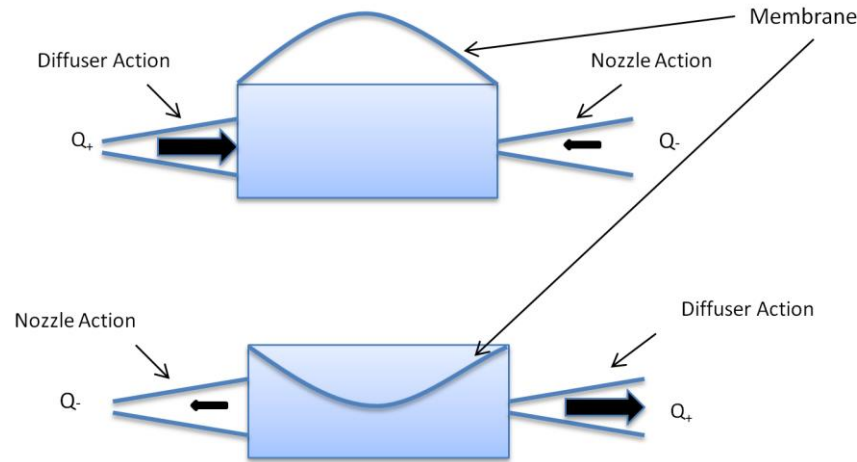


FIG 2-6- Flow rectification in a valveless micropump: (a) expansion mode (increasing volume of the pumping chamber) and (b) contraction mode (decreasing volume of the pumping chamber). The thicker arrows imply higher volume flow rates

2.2.1.1 Nozzle-diffuser elements

The volume flow rate of a valveless micropump depends on the rectification efficiency of the pump among other factors (such as amplitude and frequency of operation of the diaphragm). The rectification efficiency, ϵ , is the ratio of the volume of net fluid pumped to that crossing (entering or leaving) the pump in a given interval of time ($\epsilon = (Q_+ - Q_-) / (Q_+ + Q_-)$). The rectification efficiency of nozzle-diffuser micropumps reported in the literature is very low, generally between 0.01 and 0.2. Since the rectification efficiency of these micropumps depends on the flow directing ability of the nozzle-diffuser elements, many studies have been directed at better understanding the fluid dynamic behavior and the flow rectification properties of nozzle-diffuser elements [6, 31, 39-44].

Different shapes of nozzle-diffuser elements have been considered in the literature. They can be broadly classified as spatial and planar. Spatial diffusers can be further divided into conical and pyramidal as shown in Fig 2-7.

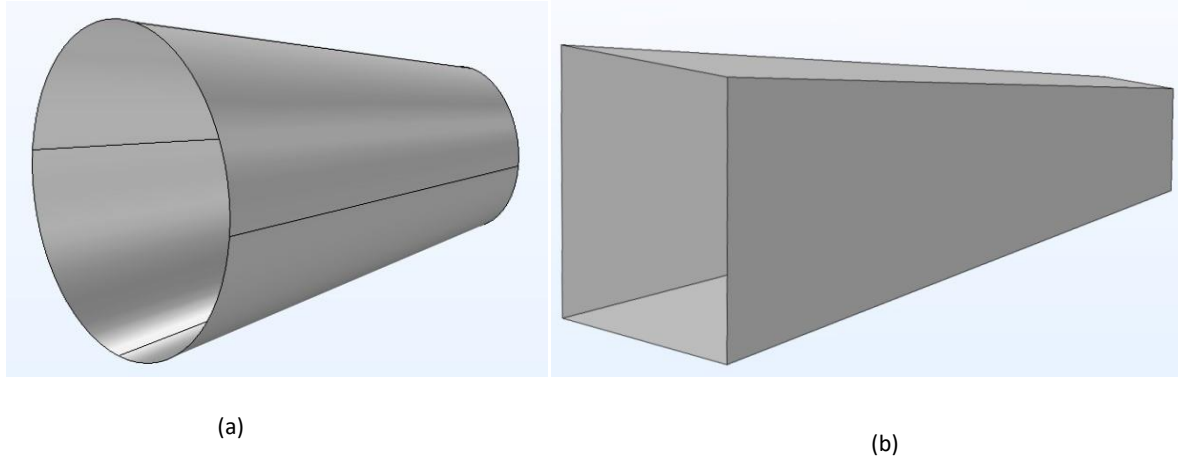


FIG 2-7- Schematic of (a) conical, (b) pyramidal nozzle-diffuser elements.

2.2.1.2 Theoretical Analysis

Pressure Loss Coefficient-

The pressure loss coefficient for flows through a gradually contracting nozzle, a gradually expanding diffuser, or a sudden expansion or contraction in an internal flow system is defined as the ratio of pressure drop across the device to the velocity head upstream of the device.

$$K = \frac{\Delta p}{\frac{\rho v^2}{2}} \quad (2.4)$$

For flow through a gradually expanding diffuser (Fig. 2-8) or a gradually contracting nozzle, the pressure loss coefficient can be calculated as follows. For flow in the diffuser direction (from cross-section a to b in Fig. 2-8), the incompressible steady-flow energy equation reduces to-

$$p_a + \frac{1}{2} \rho v_a^2 = p_b + \frac{1}{2} \rho v_b^2 + \Delta p_d \quad (2.5)$$

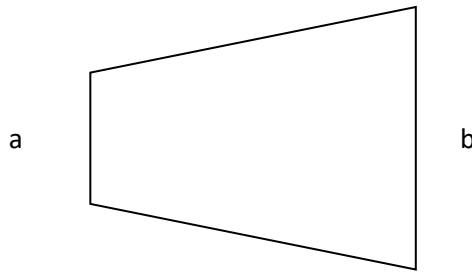


FIG 2-8- *Schematic of gradually expanding nozzle*

Hence, the pressure loss coefficient can be written as-

$$K_d = \frac{\Delta p}{\frac{\rho v^2}{2}} = \frac{p_a - p_b}{\rho v_a^2/2} + (1 - \frac{v_b^2}{v_a^2}) \quad (2.6)$$

Introducing the pressure recovery coefficient, $C_p = \frac{p_b - p_a}{\rho v_a^2/2}$, and using continuity equation

$A_a v_a = A_b v_b$, K_d for spatial diffusers (conical and pyramidal) can be written as-

$$K_d = 1 - \frac{d_a^4}{d_b^4} - C_p \quad (2.7)$$

since, $A \propto d^2$.

Hence for a given diffuser geometry, the pressure loss coefficient can be calculated from the pressure drop and the mean velocity at the neck. Similarly, for flow in the nozzle direction (from cross-section b to a in Fig. 2-8), the pressure loss coefficient is given by-

$$K_n = \frac{\Delta p_n}{\frac{\rho v_b^2}{2}} \quad (2.8)$$

Pressure loss coefficients for flow through sudden expansions and contractions can be calculated similarly.

Diffuser Efficiency

The diffuser efficiency of a nozzle-diffuser element is defined as the ratio of the total pressure loss coefficient for flow in the nozzle direction to that for the flow in the diffuser direction.

$$\eta = \frac{K_{n,t}}{K_{d,t}} \quad (2.9)$$

Hence, $\eta > 1$ will cause a pumping action in the diffuser direction (Fig. 2-6) in a valveless micropump, while $\eta < 1$ will lead to pumping action in the nozzle direction. The case where $\eta = 1$ corresponds to equal pressure drops in both the nozzle and the diffuser directions, leading to no flow rectification.

In Eq. (2.9), the total pressure loss coefficients for both the diffuser and nozzle directions can be divided into three parts: (i) losses due to sudden contraction at the entrance, (ii) losses due to gradual contraction or expansion through the length of the nozzle-diffuser, and (iii) losses due to sudden expansion at the exit. The total pressure drop at the diffuser thus can be written as-

$$\Delta p_{d,t} = \Delta p_{d,en} + \Delta p_d + \Delta p_{d,ex} \quad (2.10)$$

Therefore, the total pressure loss coefficient for the diffuser can be calculated as-

$$K_{d,t} = K_{d,en} + K_d + K_{d,ex} \frac{A_a^2}{A_b^2} \quad (2.11)$$

Similarly, the total pressure loss coefficient for the nozzle (with respect to pressure head at the neck) is-

$$K_{n,t} = (K_{n,en} + K_n) \frac{A_a^2}{A_b^2} + K_{n,ex} \quad (2.12)$$

Therefore, diffuser efficiency can be written as-

$$\eta = \frac{K_{n,t}}{K_{d,t}} = \frac{(K_{n,en} + K_n)(A_a^2/A_b^2) + K_{n,ex}}{K_{d,en} + K_d + K_{d,ex}(A_a^2/A_b^2)} \quad (2.13)$$

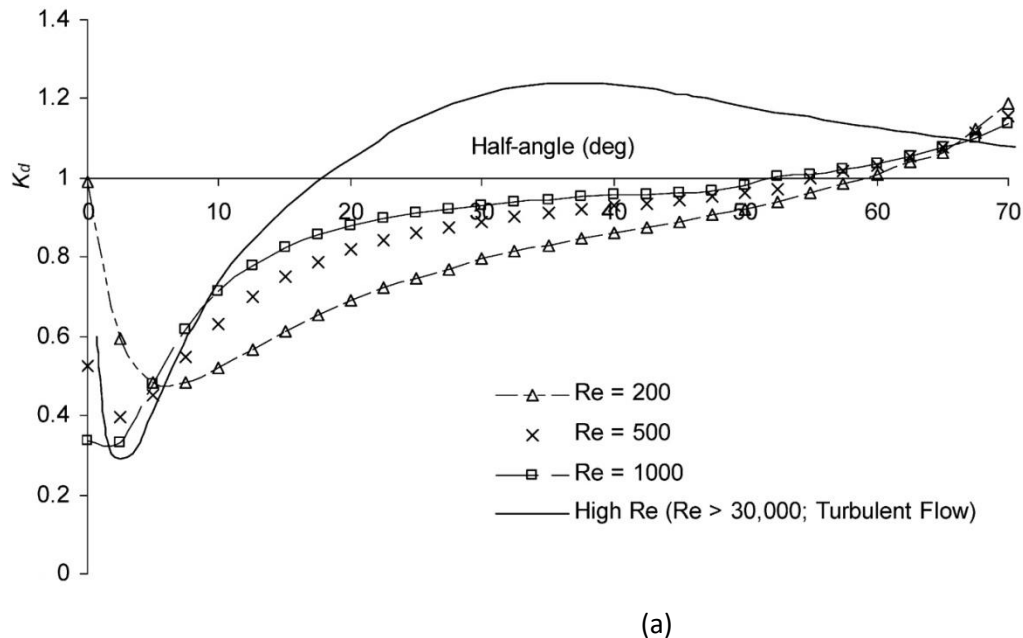
Flow Rectification Efficiency

The flow rectification efficiency of a valveless micropump is the measure of the ability of the pump to direct the flow in one preferential direction. It can be expressed as-

$$\varepsilon = \frac{Q_+ - Q_-}{Q_+ + Q_-} \quad (3.0)$$

in which Q is flow rate and subscripts + and - refer to flow in the forward and the backward directions, respectively. A higher ε corresponds to better flow rectification. In particular, when there is no flow rectification, equal amounts of fluid move in both directions and $\varepsilon = 0$, while for perfect rectification, flow is only in one direction and $\varepsilon = 1$. The flow rectification efficiency of a valveless micropump is related to the diffuser efficiency of the nozzle-diffuser elements. As the diffuser efficiency departs from a value of 1, i.e. as the difference between $K_{n,t}$ and $K_{d,t}$ increases, ε for the micropump also increases.

Considering these theories, several studies have been undergone to understand the flow behavior of nozzle-diffuser elements at low Reynolds numbers. It has been shown in [45], the variation of pressure losses with the diffuser angle through gradually expanding diffusers, for conical and planar diffuser cross-section shapes. The analysis considers flow Reynolds numbers of 200, 500 and 1000.



(a)

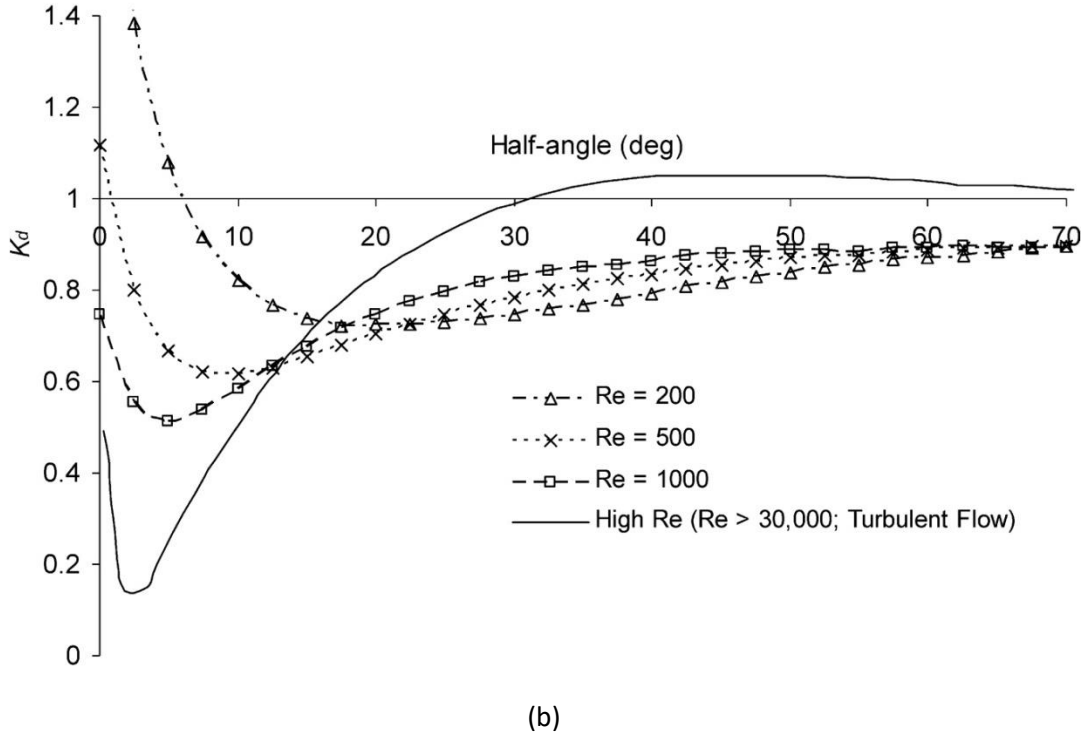


FIG 2-9- Plot of variation of pressure loss coefficient in a conical diffuser with half-angle of the cone for $Re = 200, 500, 1000$ and $>30,000$ for (a) fully developed inlet boundary layer and (b) thin inlet boundary layer.[45]

It was seen that for both inlet flow conditions, the variation of K_d with cone angle follows the general trend observed for high Reynolds number flows ($R_e > 30,000$), although K_d values obtained here are greater and smaller than those for high Reynolds number flows at small and large cone half-angles, respectively. Moreover, at the low Reynolds numbers considered, K_d for a given diffuser angle varies significantly with Reynolds number, especially at small cone angles. In contrast, K_d for high Reynolds number flows does not vary with Reynolds number. For small cone angles, the loss coefficients decrease with increasing Re , while at large cone angles, they increase with increasing Re . The high loss coefficients for small diffuser angles at low Re are believed to be due to the dominance of viscous forces in these very ordered flows. As the cone angle increases, flow separation occurs, which is associated with higher loss coefficients (higher than the viscous contributions). Since flow separation is more dominant for higher Re , loss coefficients at the larger cone angles are also greater for larger Re . Comparing the numerical values of K_d for the fully developed and thin inlet boundary layer flows, it can be observed that

for small cone angles, K_d is smaller for the fully developed boundary layer and vice versa (K_d is smaller for the thin inlet boundary layer flows for large cone angles). Also, this behavior is peculiar to low Reynolds number flow. At high Reynolds numbers, K_d for the fully developed inlet boundary layer flow is smaller than that for thin inlet boundary layers for all cone angles. The higher K_d for thin inlet boundary layer flows might be attributable to an additional pressure drop due to the boundary layer development in these flows, which is absent for fully developed inlet boundary layers.

So, tuning the value of K_d , an optimal geometry of the nozzle diffuser can be seen. It was seen in other studies [46, 47], that a half angle of 5° served as the optimal diffuser angle for the pump system. This conclusion is widely adopted as the design rule for decades, and most of the reported valve-less micropumps obey such rule till now.

It can be seen in Fig 2-10, when micropump is in suction mode, it is clearly shown that turbulence emerges in the interfacial area of micropump chamber and nozzle. This turbulence may help to block the fluid flows from outlet. However, the fluid flow from inlet has encounters small resistance. Therefore, the fluid flow into pump chamber through inlet is larger than outlet. For the same reason, when micropump is in pumping mode, the turbulence prevents the fluid flows to inlet. The fluid flow out through outlet is larger than inlet. Hence, micropump produces unidirectional flow. In general, both diffuser/nozzle, pump chamber and inlet/outlet chamber are make contribution to generate net flow.

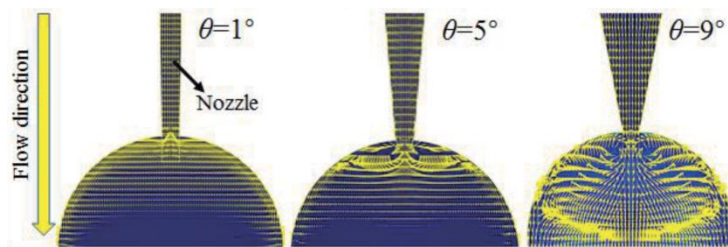


FIG 2-10- *The computation domain of micropump- simulation velocity field for $\theta=1^\circ$, $\theta=5^\circ$, and $\theta=9^\circ$* [46]

Again in [47], it was seen that the optimal angle of diffuser was with a half angle of 4.5° . So, complying with these theories, the micropump in this project was designed keeping in

considerations of the values of Reynolds number of the fluid along with the optimal geometry considerations.

2.3 Peristaltic Micropumps

Mechanical pumps can handle a large variety of fluids, but often involve complicated structures and present integration challenges, as is evident in rotary pumps (requiring bearings) and some diaphragm pumps (requiring check valves). However, peristaltic pumps are a class of mechanical pumps that are relatively simple in structure and suitable for miniaturization. Moreover, electrostatic actuation is well suited to peristaltic pumping. It consumes much less power than other actuation mechanisms (e.g., thermopneumatic actuation) while still delivering reasonable pumping flow rates and pressures. Compared to piezoelectric actuation, electrostatic actuation can produce more displacement without complicated fabrication, leading to a higher expansion/compression ratio. Since microfluidic systems are especially useful for biological applications, the low-power and low-temperature operation of electrostatic pumping is even more attractive.

Peristalsis theory, developed about 40 years ago [23, 24], considers fluid motion in an infinitely long tube whose wall contracts in a prescribed traveling wave form. As such, it does not apply to peristaltic micropumps whose channel wall motion is coupled to fluid flow. Analytical and numerical calculations of static diaphragm deflections and pumping stroke volumes have been considered for piezoelectric peristaltic micropumps [25]. Also restricted to static characteristics, piezoelectric [4] and electrostatic [26] peristaltic pumps have been modeled by assuming the flow rate to be proportional to the actuation frequency and stroke volume, which is determined from the diaphragm motion by ignoring its interaction with fluid flow. More recently, a lumped-parameter analysis has been reported for diaphragmbased micropumps working peristaltically using active valves driven by general actuation schemes [27]. While pumping dynamics is considered, the coupling of viscous fluid flow and diaphragm motion is not adequately accounted for.

2.3.1 Peristaltic pump design

A schematic of the surface-micromachined peristaltic micropump is shown in Fig. 2-11 [10]. The pump has three pumping cells connected in series. Essential components of each pumping cell include a fluid chamber, an electrode gap and a moving diaphragm that separates them. The electrode gap lies between a fixed ground electrode located on the substrate, and a moving electrode embedded in the diaphragm. Air in the electrode gap is vented to the ambient through a venting hole. The fluid chambers in the three pumping cells are connected in series. When an actuation voltage is applied between the two electrodes, electrostatic force will pull the diaphragm downward and cause expansion of the fluid chamber volume. When the pumping cells are actuated using a three-phase peristaltic sequence [6], the resulting peristaltic motion will induce pumping of the fluid inside the chambers.

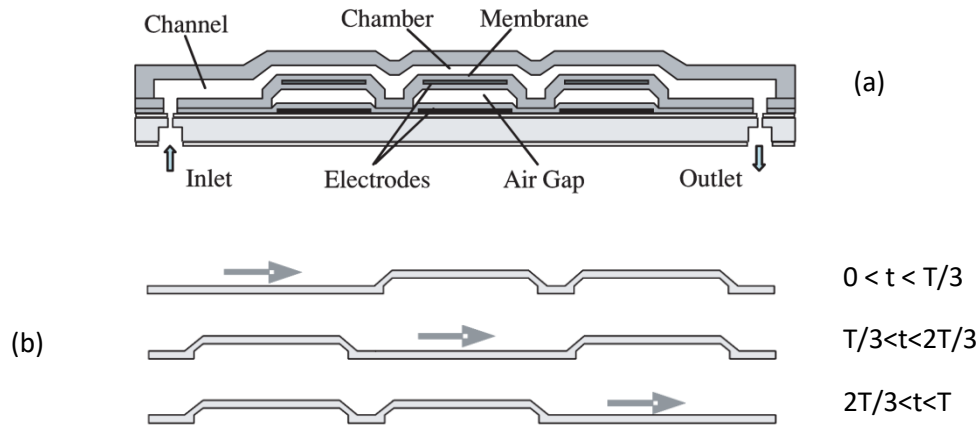


FIG 2-11- (a) Schematic of the peristaltic pump. (b) Actuation in a period T .[48]

2.3.2 Pumping cell representation

This section considers a representation of the individual pumping cells, which will then be used to construct a model for the entire pump. The upstream, middle and downstream pumping cells, including their associated diaphragms, fluid chambers and electrode gaps, are given indices $i=1,2,3$ respectively. They are assumed to have identical shape and dimensions. These include the fluid chamber height (h) and electrode gap thickness (d), both measured in the absence of diaphragm deflection. In addition, the fluid chamber, diaphragm and electrodes are assumed to have the same radius (a), and the channels connected to each chamber have equal width b . A representation of the pumping cell i is shown in figure 2-12. Here, the pressure and flow rate at

the entrance of the fluid chamber are, respectively, p_i and Q_i , and those at the exit are p_{i+1} and Q_{i+1} . Actuated with a voltage V_i , the diaphragm has deflection δ_i , which is represented by the displacement of a spring-attached rigid plate (below). Note that when V_i is periodic with frequency f , so are the pressure, flow rate and diaphragm deflection. We first consider the diaphragm deflection under electrostatic and hydrodynamic forces and then model the fluid flow in the fluid chamber.

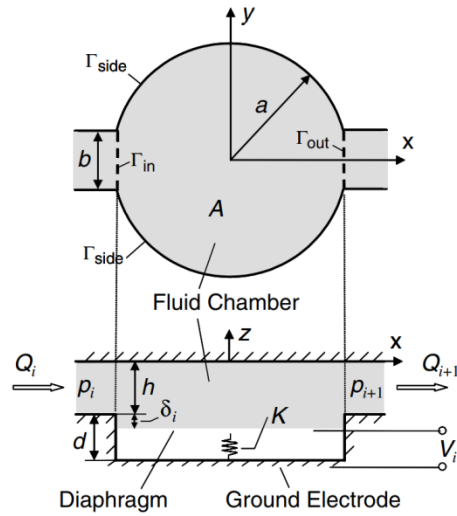


FIG 2-12- Representation of a pumping cell.[48]

2.3.2.1 Diaphragm vibrations

The diaphragm in a pumping cell vibrates elastically under the action of electrostatic and hydrodynamic forces. While the deflection varies continuously with location on the diaphragm, for a lumped-parameter representation we approximate the diaphragm as a rigid plate attached to an elastic spring with spring coefficient K (Fig 2-12), whose determination will be described below. The diaphragm deflection is then represented by the displacement of the rigid plate, δ_i . This approximation drastically simplifies the description of the diaphragm vibration as well as the associated fluid flow. In general, in addition to the electrostatic and hydrodynamic forces, the diaphragm vibration is influenced by the effects of diaphragm inertia as well as damping due to air flow in the electrode gap. However, as the electrode gap is connected to the ambient by vent holes, the air flow is largely unimpeded. Thus, air damping effects are small compared to

hydrodynamic squeeze-film damping effects (below) and can be neglected. Additionally, vibration theory [29, 30] can be used to estimate that the natural frequency of the diaphragm is about three orders of magnitude higher than the actuation frequency, which is typically below 100 Hz. This implies that the diaphragm inertia is also negligible. Thus, the spring-attached plate is approximately massless and undergoes quasistatic vibration, which is governed by the following algebraic equation:

$$K \delta_i = F_i^{electro} + F_i^{hydro} \quad (3.1)$$

F_i^{hydro} is the hydrodynamic force as will be considered in the next subsection and $F_i^{electro}$ is the electrostatic actuation force given by-

$$F_i^{electro} = \frac{\epsilon_0 V_i^2 A}{2(d_{eff} - \delta_i)^2} \quad (3.2)$$

Here, ϵ is the free-space permittivity, $A = \pi a^2$ is the approximate diaphragm area and $d_{eff} = d + t_p/\epsilon_p$ is the effective separation of the moving and ground electrodes with t_p and ϵ_p being the thickness and dielectric constant of the insulation layers between the electrodes.

The spring coefficient (K), representing the stiffness of the diaphragm, consists of contributions from diaphragm bending, in-plane pretension and stretching of the diaphragm's middle surface [30]. The bending effects are characterized by the plate's bending rigidity $D = Et_m^3/12(1 - \nu^2)$, and pretension by the in-plane force per unit length $N = \sigma t_m$, where E is the Young's Modulus, ν is the Poisson's ratio, σ is the in-plane residual stress that results from the temperature history of the fabrication process, and a and t_m are the diaphragm radius and thickness. For simplicity middle-surface stretching of the diaphragm is neglected, so that K is approximately a constant. For the particular case of an electrostatically actuated diaphragm, K can be approximately determined in a way consistent with the determination of the critical voltage, V_p , at which the electrostatic pull-in instability occurs. That is, while the pull-in voltage is $V_p = (\frac{8Kd_{eff}^3}{27\epsilon_0 A})^{\frac{1}{2}}$ for the spring-attached rigid plate, it is $V_p = (\frac{4.8Nd_{eff}^3}{\lambda\epsilon_0 A})^{\frac{1}{2}}$ for the diaphragm, where $\lambda = 1 + 2^{(1 - \cosh q)/(q \sinh q)} < 1$ with $q = 0.825(\frac{Na^2}{D})^{\frac{1}{2}}$. The spring coefficient is chosen as- $K = \frac{16.4 N}{\lambda}$ so that these two expressions will consistently give the same pull-in

voltage. Note that in the cases $\lambda \rightarrow 1$ and $\lambda < 1$, diaphragm stiffness is predominantly due to pretension and bending effects, respectively.

2.3.2.2 Fluid Flow

In a fluid chamber, the diaphragm vibration induces the motion of the thin fluid film confined between the narrow gap formed by the diaphragm and the chamber ceiling. In reality, the fluid film thickness varies continuously with location due to the diaphragm's continuous deflection. However, the approximation of the diaphragm as a spring-attached rigid plate results in a fluid film with uniform thickness, which is only a function of time, t . The dynamics of this fluid film is now considered to obtain an expression for the hydrodynamic force F_i^{hydro} as well as a relationship relating the pressures and flow rates at the entrance and exit of the fluid chamber.

Since the fluid film thickness is small compared with the diaphragm radius (i.e., $h/a < 1$), its motion can be represented by use of lubrication theory [49]. To begin with, let f be the diaphragm's vibration frequency. Then, the flow velocity in the z-direction has a characteristic value of $\omega_0 = \omega(d_{eff}/3)$, where $\omega = 2\pi f$ is the circular frequency and $d_{eff}/3$, the diaphragm displacement at which electrostatic pull-in instability occurs [50], is taken to be the diaphragm's characteristic displacement. We next define an out-of-plane Reynolds number $Re_z = \rho\omega_0 h/\mu$ and an in-plane Reynolds number $-Re = \left(\frac{\rho u_0 h}{\mu}\right) \left(\frac{h}{a}\right)$, where ρ and μ are the fluid density and dynamic viscosity, respectively. When these Reynolds numbers are of order h/a or smaller, inertial effects in the flow can be ignored when compared with viscous and pressure effects [49]. Also, unsteady flow and gravity effects can be neglected if the squeeze number $\sigma_s = \frac{\rho\omega h^2}{\mu} = Re_z \left(\frac{3h}{d_{eff}}\right)$ and the dimensionless parameter $\rho gh^2/(\mu\mu_0)$ are of order h/a or smaller. With these conditions hold, the classical Reynolds equation of lubrication theory [34] adequately describes the hydrodynamics of the fluid film. In the coordinate frame shown in Fig 2-12, this equation takes the form-

$$\nabla \cdot ((h + \delta_i) 3 \nabla p) = 12 \mu \delta_i$$

$$p|_{\tau_{in}} = p_i \quad p|_{\tau_{out}} = p_{i+1} \quad \frac{\partial p}{\partial n}|_{\tau_{side}} = 0 \quad (3.3)$$

Where, the pressure, p , inside the chamber is assumed not to vary along the fluid film thickness and ∇ is the planar gradient operator.

Here, the equation is defined over the planar domain corresponding to the fluid chamber, which approximately has the same area, A , as the diaphragm. The fluid film thickness, given by $h + \delta_i$ in the presence of diaphragm deflection, does not vary with in-plane coordinates x and y . As shown in the appendix, this greatly simplifies the solution of equation (3.3). In particular, if the fluid chamber is symmetric about the y -axes, we obtain the hydrodynamic force-

$$F_i^{hydro} = - \frac{\alpha \mu l^2 A}{(h+\delta_i)^3} \delta_i + \frac{1}{2} \beta (p_i + p_{i+1}) A \quad (3.4)$$

And, the flow rates at the chamber inlet and outlet-

$$Q_{i+1}^i = \pm \frac{1}{2} A \delta_i + \frac{\gamma (h+\delta_i)^3}{12 \mu} (p_i - p_{i+1}) \quad (3.5)$$

Here, the coefficients α , β and γ are given by-

$$\begin{aligned} \alpha &= \frac{12}{\bar{A}} \int_{\bar{A}} \emptyset d\bar{A} & \beta &= \frac{2}{\bar{A}} \int_{\bar{A}} \varphi d\bar{A} \\ \gamma &= \int_{\Gamma_{in}} \frac{\partial \varphi}{\partial \bar{n}} |_{\Gamma_{in}} d\bar{\Gamma} \end{aligned} \quad (3.6)$$

Where, the functions \emptyset and φ are solutions to the following normalized equations:

$$\begin{cases} \overline{\nabla^2} \emptyset = -1 \\ \emptyset |_{\tau_{in}} = 0, \emptyset |_{\tau_{out}} = 0, \frac{\partial \emptyset}{\partial \bar{n}} |_{\tau_{side}} = 0 \end{cases} \quad \text{and} \quad \begin{cases} \nabla^2 \varphi = 0 \\ \varphi |_{\tau_{in}} = 1, \varphi |_{\tau_{out}} = 0, \frac{\partial \varphi}{\partial \bar{n}} |_{\tau_{side}} = 0 \end{cases} \quad (3.7)$$

Here, \bar{A} also denotes the fluid chamber domain scaled by l , with $\overline{\Gamma_{in}}$, $\overline{\Gamma_{out}}$ and $\overline{\Gamma_{side}}$ denoting the corresponding boundaries scaled by l . It is important to note that these coefficients need to be calculated only once for pumping cells of the same shape but different size.

In equation (3.4), the first term accounts for the squeezefilm damping effects from interactions of viscous fluid flow and diaphragm motion [49] and the second term represents the hydrostatic effects of inlet and outlet pressures. Similarly, in equation (3.5), the first and second terms account for flow rate contributions from the diaphragm motion and inlet–outlet pressure

difference, respectively. It can be observed that in the absence of diaphragm motion, this equation reduces to the classical relationship for Poiseuille flow.

Equation (3.5) provides an integral description of fluid flow in the chamber. Meanwhile, a differential description of diaphragm vibration can be obtained by substituting equation (3.4) into equation (3.1):

$$K \delta_i + \frac{\alpha \mu l^2 A}{(h+\delta_i)^3} \delta_i = \frac{\epsilon_0 V_i^2 A}{2(d_{eff}-\delta_i)^2} + \frac{1}{2} \beta (p_i + p_{i+1}) A \quad (3.8)$$

2.3.3 System-level pump model

We can now represent the entire peristaltic pump as a system. This system consists of components including the individual pumping cells and loads connected in series, whose behavior is given by component-level representations described in the previous section. Specifically, each individual pumping cell i ($i = 1, 2, 3$) is represented by equations (3.5) and (3.8), which relate six basic variables and parameters characterizing fluid flow and diaphragm motion in the cell: p_i , p_{i+1} , Q_i , Q_{i+1} , δ_i , and V_i . The loads upstream and downstream of the pump are typically in the form of microchannels. Neglecting unsteady flow effects and provided the channel length is long compared with the channel's cross-sectional dimensions, such channels can be represented respectively as pure flow resistances, R_{in} and R_{out} , at the pump inlet and outlet.

These flow resistances, based on elementary considerations of Poiseuille flow, relate the pressures and flow rates by the following algebraic equations-

$$-p_1 = R_{in} Q_1 \quad \text{and} \quad p_4 - p_{back} = R_{out} Q_4 \quad (3.9)$$

where p_{back} is the back pressure at the outlet. The pressure at the pump inlet is set to zero without loss of generality.

The pump to be designed will follow the following set of equations from equation (3.5), equation (3.8) and equation (3.9).

Note that the model is based on first principles and can be evaluated directly from the device's geometric and material properties without using any experimentally identified parameters.

REFERENCES

- [1] P. Gravesen, J. Brandebjerg, and O. Søndergaard Jensen, "Microfluidics - a review," *Journal of Micromechanics and Microengineering*, vol. 3 (1993) 168-182
- [2] S. Shoji and M. Esashi, "Microflow devices and systems," *Journal of Micromechanics and Microengineering*, vol. 4 (1994) 157-171.
- [3] J. G. Smits, "Piezoelectric Micropump with Three Valves Working Peristaltically," *Sensors and Actuators*, vol. A21-A23 (1990) 203-206.
- [4] H. T. G. van Lintel, F. C. M. van den Pol, and S. Bouwstra, "A piezoelectric micropump based on micromachining in silicon," *Sensors and Actuators*, vol. 15 (1988) 153-167.
- [5] R. Zengerle, S. Kluge, M. Richter, and A. Richter, "A Bidirectional Silicon Micropump," IEEE 8th International Workshop on Micro Electro Mechanical Systems (MEMS'95), Amsterdam, the Netherlands, Jan. 29 - Feb. 2, 1995, pp. 19-24.
- [6] E. Stemme and G. Stemme, "A Valve-less Diffuser/Nozzle based Fluid Pump," *Sensors and Actuators*, vol. A39 (1993) 159-167
- [7] C. H. Ahn and M. G. Allen, "Fluid Micropumps Based on Rotary Magnetic Actuators," IEEE 8th International Workshop on Micro Electro Mechanical Systems (MEMS'95), Amsterdam, the Netherlands, Jan. 29-Feb. 2, 1995, pp. 408-412
- [8] Bernstein, J.J., S.L. Finberg, K. Houston, L.C. Niles, H.D. Chen, L.E. Cross, K.K. Li, and K. Udayakumar, Micromachined high frequency ferroelectric sonar transducers. *Ultrasonics, Ferroelectrics and Frequency Control, IEEE Transactions on*, 1997. vol. 44: p. 960–969.
- [9] Luginbuhl, P., S.D. Collins, G.-A. Racine, M.-A. Gretillat, N.F. De Rooij, K.G. Brooks, and N. Setter, Microfabricated lamb wave device based on PZT sol-gel thin film for mechanical transport of solid particles and liquids. *Microelectromechanical Systems, Journal of*, 1997. vol. 6: p. 337–346.
- [10] Li, H.Q., D.C. Roberts, J.L. Steyn, K.T. Turner, O. Yaglioglu, N.W. Hagood, S.M. Spearing, and M.A. Schmidt, Fabrication of a high frequency piezoelectric microvalve. *Sensors and Actuators A: Physical*, 2004. vol. 111: p. 51–56.

- [11] Wang, L.-P., R.A. Wolf, Y. Jr. Wang, K.K. Deng, L. Zou, R.J. Davis, and S. Trolier-McKinstry, Design, fabrication, and measurement of high-sensitivity piezoelectric microelectromechanical systems accelerometers. *Microelectromechanical Systems, Journal of*, 2003. vol. 12: p. 433–43
- [12] DeVoe, D.L. and A.P. Pisano, Surface micromachined piezoelectric accelerometers (PiXLs). *Microelectromechanical Systems, Journal of*, 2001. vol. 10: p. 180–186
- [13] Ried, R.P., E.S. Kim, D.M. Hong, and R.S. Muller, Piezoelectric microphone with on-chip CMOS circuits. *Microelectromechanical Systems, Journal of*, 1993. vol. 2: p. 111–120.
- [14] Lee, S.S., R.P. Ried, and R.M. White, Piezoelectric cantilever microphone and microspeaker. *Microelectromechanical Systems, Journal of*, 1996. vol. 5: p. 238–242,
- [15] Mescher, M.J., M.L. Vladimer, and J.J. Bernstein, A novel high-speed piezoelectric deformable varifocal mirror for optical applications. presented at Micro Electro Mechanical Systems, 2002. The Fifteenth IEEE International Conference on, 2002.
- [16] Vig, J.R., R.L. Filler, and Y. Kim, Chemical sensor based on quartz microresonators. *Microelectromechanical Systems, Journal of*, 1996. vol. 5: p. 138–140.
- [17] Foundation on MEMS, Chang Liu
- [18] R. G. Gilbertson and J. D. Busch, “A Survey of Micro-Actuator Technologies for Future Spacecraft Missions,” Practical Robotic Interstellar Flight: Are We Ready?, New York City, August 29 - September 1, 1994.
- [19] Thorsén, Anders. (1998). Valveless Diffuser Micropumps.
- [20] C. H. Ahn and M. G. Allen, “Fluid Micropumps Based on Rotary Magnetic Actuators,” IEEE 8th International Workshop on Micro Electro Mechanical Systems (MEMS'95), Amsterdam, the Netherlands, Jan. 29-Feb. 2, 1995, pp. 408-412.
- [21] J. G. Smits, “Piezoelectric Micropump with Three Valves Working Peristaltically,” Sensors and Actuators, vol. A21-A23 (1990) 203-206.
- [22] H. Mizoguchi, M. Ando, T. Mizuno, T. Takagi, and N. Nakajima, “Design and fabrication of light driven micropump,” IEEE 5th International Workshop on Micro Electro Mechanical Systems (MEMS'92), Travemünde, Germany, February 4-7, 1992, pp. 31-36

- [23] H. T. G. van Lintel, F. C. M. van den Pol, and S. Bouwstra, "A piezoelectric micropump based on micromachining in silicon," *Sensors and Actuators*, vol. 15 (1988) 153-167.
- [24] F. C. M. van de Pol, H. T. G. van Lintel, M. Elwenspoek, and J. H. J. Fluitman, "A Thermopneumatic Micropump Based on Micro-engineering Techniques," *Sensors and Actuators*, vol. A21-A23 (1990) 198-202.
- [25] S. Shoji, S. Nakafawa, and M. Esashi, "Micropump and sample-injector for integrated chemical analyzing systems," *Sensors and Actuators*, vol. A21-A23 (1990) 189-192.
- [26] R. Zengerle, A. Richter, and H. Sandmaier, "A micromembrane pump with electrostatic actuation," IEEE 5th International Workshop on Micro Electro Mechanical Systems (MEMS'92), Travemünde, Germany, February 4-7, 1992, pp. 19-24.
- [27] T. S. J. Lammerink, M. Elwenspoek, and J. H. J. Fluitman, "Integrated micro-liquid dosing system," IEEE 6th International Workshop on Micro Electro Mechanical Systems (MEMS'93), Fort Lauderdale, Florida, USA, February 7-10, 1993, pp. 254-259.
- [28] E. Stemme and G. Stemme, "A Valve-less Diffuser/Nozzle based Fluid Pump," *Sensors and Actuators*, vol. A39 (1993) 159-167.
- [29] T. Gerlach, "A simple micropump employing dynamic passive valves made in Si," *MICRO SYSTEM Technologies '94*, Berlin, Germany, October 19-21, 1994, pp. 1025- 1034.
- [30] T. Gerlach, M. Schuenemann, and H. Wurmus, "A new micropump principle of the reciprocating type using pyramidal micro flow channels as passive valves," *Journal of Micromechanics and Microengineering*, vol. 5 (1995) 199-201.
- [31] T. Gerlach and H. Wurmus, "Working principle and performance of the dynamic micropump," *Sensor and Actuators*, vol. A50 (1995) 135-140.
- [32] R. Zengerle, S. Kluge, M. Richter, and A. Richter, "A Bidirectional Silicon Micropump," IEEE 8th International Workshop on Micro Electro Mechanical Systems (MEMS'95), Amsterdam, the Netherlands, Jan. 29 - Feb. 2, 1995, pp. 19-24.
- [33] M. Stehr, S. Messner, H. Sandmaier, and R. Zengerle, "A New Micropump with Bidirectional Fluid Transport and Selfblocking Effect," IEEE 9th International Workshop on Micro Electro Mechanical Systems (MEMS'96), San Diego, California, USA, February 11-15, 1996, pp. 485-490.

- [34] K.-P. Kämper, J. Döpper, W. Ehrfeld, and S. Oberbeck, “A Self-filling Low-cost Membrane Micropump,” IEEE 11th International Workshop on Micro Electro Mechanical Systems (MEMS'98), Heidelberg, Germany, Jan. 25-29, 1998, pp. 432-437.
- [35] R. Linneman, P. Woias, C.-D. Senfft, and J. A. Ditterich, “A Self-priming and Bubbletolerant Piezoelectric Silicon Micropump for Liquids and Gases,” IEEE 11th International Workshop on Micro Electro Mechanical Systems (MEMS'98), Heidelberg, Germany, Jan. 25-29, 1998, pp. 532-537.
- [36] F. C. M. van de Pol, Thesis: A pump based on micro-engineering techniques, University of Twente, Enschede, the Netherlands, 1989
- [37] L. Smith, “Micromachined nozzles fabricated with replicative method,” Micromechanics Europe 1990 (MME '90), Berlin, Germany, 26-27 November, 1990, pp. 53-57.
- [38] E. Stemme and G. Stemme, “Valve-Less Fluid Pump,” Swedish Patent Appl. No. 9 300 604-7, 1993.
- [39] X.N. Jiang, Z.Y. Zhou, X.Y. Huang, Y. Li, Y. Yang, C.Y. Liu, Micronozzle/diffuser flow and its application in micro valveless pumps, *Sens. Actuators A: Phys.* 70 (1998) 81–87.
- [40] A. Olsson, G. Stemme, E. Stemme, Diffuser-element design investigation for valve-less pumps, *Sens. Actuators A: Phys.* 57 (1996) 137–143.
- [41] M. Heschel, M. Mullenborn, S. Bouwstra, Fabrication and characterization of truly 3-D diffuser/nozzle microstructures in silicon, *J. Microelectromechan. Syst.* 6 (1997) 41–47.
- [42] M. Koch, A.G.R. Evans, A. Brunschweiler, The dynamic micropump driven with a screen printed PZT actuator, *J. Micromechan. Microeng.* 8 (1998) 119–122.
- [43] T. Gerlach, Microdiffusers as dynamic passive valves for micropump applications, *Sens. Actuators A: Phys.* 69 (1998) 181–191
- [44] A. Olsson, G. Stemme, E. Stemme, Numerical and experimental studies of flat-walled diffuser elements for valveless micropumps, *Sens. Actuators A: Phys.* 84 (2000) 165–175.
- [45] Vishal Singhal, Suresh V. Garimella, Jayathi Y. Murthy, Low Reynolds number flow through nozzle-diffuser elements in valveless micropumps, *Sensors and Actuators A: Physical*, Volume 113, Issue 2, 2004, Pages 226-235

- [46] T. Wang et al., "Numerical and Experimental Study of Valve-Less Micropump Using Dynamic Multiphysics Model," 2018 IEEE 13th Annual International Conference on Nano/Micro Engineered and Molecular Systems (NEMS), 2018, pp. 300-303, doi: 10.1109/NEMS.2018.8557014.
- [47] Gidde, R.R., Pawar, P.M. & Dhamgaye, V.P. Fully coupled modeling and design of a piezoelectric actuation based valveless micropump for drug delivery application. *Microsyst Technol* **26**, 633–645 (2020).
- [48] Lin, Qiao & Yang, Bozhi & Xie, Jun & Tai, Yu-Chong. (2007). Dynamic simulation of a peristaltic micropump considering coupled fluid flow and structural motion. *Journal of Micromechanics and Microengineering*. 17. 10.1088/0960-1317/17/2/006.
- [49] Hamrock B J 1994 Fundamentals of Fluid Film Lubrication (New York, NY: McGraw-Hill)
- [50] Osterberg P M and Senturia S D 1997 M-test: a test chip for MEMS material property measurement using electrostatically actuated test structures *J. Microelectromech. Syst.* **6** 107–18

CHAPTER 3

Concept for applications of Micropumps in different Bio-Med domains.

3.1 Application of Nozzle/Diffuser Micropump in NPWT

Vacuum Assisted Closure (VAC) Therapy or the Negative Pressure Wound Therapy is established in literature as we have seen in Chapter 1. Application of NPWT on different wounds is common nowadays but, the main issue such patient faces is the easy availability of the machine and also due the large size of the machine, patient is bound to a certain place for longer time.

Wounds/cuts are not only subjected to outer part of the body but also during surgery, internal bleeding happens which can't be stopped using classical mechanism or classical NPWT.

The MEMS based nozzle/diffuser micropump will thus be introduced to solve this problem. Due to its small size, micropumps can be applied to cuts which are not only in the outer part of the body but also in the inside.

Major blood vessel injury is a true emergency during endoscopic procedures. Proper technique for inserting the Veress needle, laparoscopic cannula, and open cannulas can prevent most accidents. If standard precautions during insertion are breached, safety shields on disposable cannula sleeves may not prevent or reduce the risk of major vessel injury. Distorted anatomy or steep Trendelenburg position may increase the risk. Retroperitoneal hematomas require exploratory laparotomy for proper assessment. Dissections around the great vessels of the pelvis require the same methods and precautions during laparoscopy as during laparotomy[1,2].

In [1] nine case reports were in detail described out of 47 cases of such injuries during endoscopy or laparoscopic surgeries. So, having a micropump serves as a great advantage to treat the wounds and heal faster.

It is essential for the micropump to apply a constant negative pressure on the wound. This can be achieved by stacked nozzle/diffuser micropumps with alternating voltage actuation. The working and schematic of such micropump is shown in Fig 3-1.

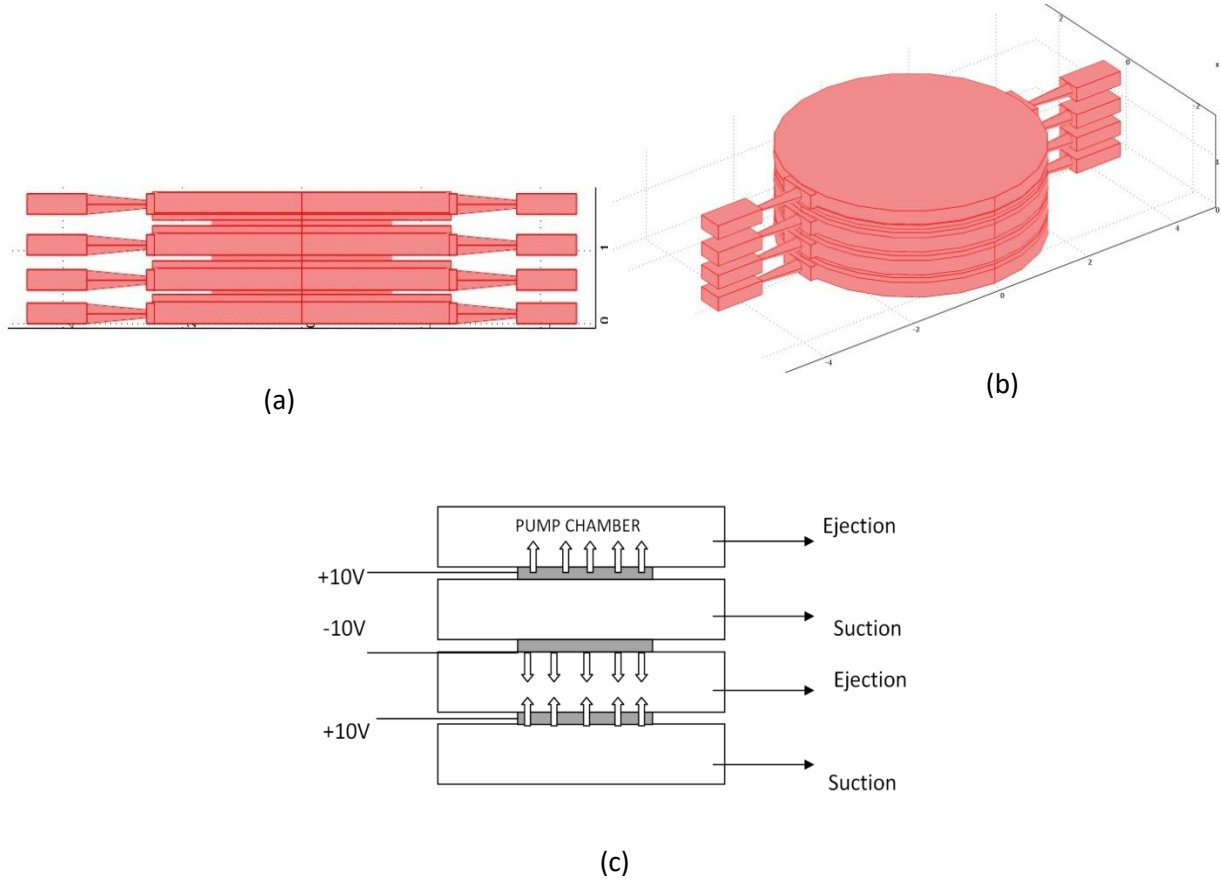


FIG 3-1- (a),(b) Schematic of the proposed micropump (c) Working Principle

3.2 Application of Peristaltic Micropump with incorporated pressure sensor for treatment of Glaucoma

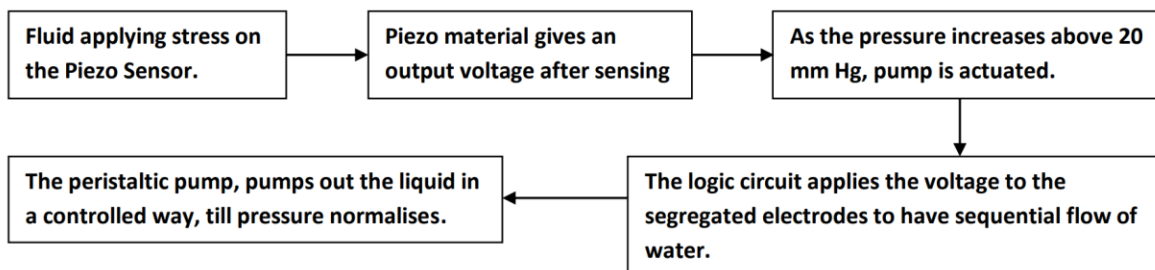
Controlling of IOP is done in today's world by inducing drug to the eye which restricts the production of ocular fluid. It can happen due to irregularities of application of drug to the eye the ocular fluid increases and thus increases the IOP. Thus, a permanent solution is required to lower the pressure and maintain at a stable pressure. For this an implantable pump is required which can sense the increase in the fluid pressure and pump out the excess fluid that can exert a high pressure on the eye membrane. For this application, the pump that is needed will have to be self-

working or autonomous without any external actuation needed. This purpose can be solved by a stacked piezoelectric pressure sensor integrated with a NEMS based peristaltic pump.

Working Principle:

We know that the normal eye pressure is 15-18mm Hg. So, a pressure higher than that will affect and increase the eye pressure. In the device, the pressure sensor will sense the increase in the eye pressure and will send a signal to the micropump. Now, comes the question of the electrostatic actuation of the micropump. Here we will use the property of piezoelectric material to generate voltage while deformed or under stress. As the Piezo sensor is deformed, due to mechanical stress, the material would produce electrostatic potential which will act as the actuation mechanism for the pump. Then an integrated logic circuit will provide the signal to the different electrodes of the peristaltic pump to pump out the liquid in a very controlled way. Now, as the pressure lowers down due to pumping, the Piezo sensor will be back from its deformed shape to normal, thus no voltage being supplied to the pump. The pump ceases to work till the eye pressure increases again. This working of the device is autonomous and without any external influence to the eye.

So, the whole device can be segregated into different parts.



The beauty of the device lies in self actuation when the pressure increases, the controlled pumping of the fluid out of the eye thus lowering the ocular pressure when needed and the bio-compatibility. The pump is shown in Fig 3-2.

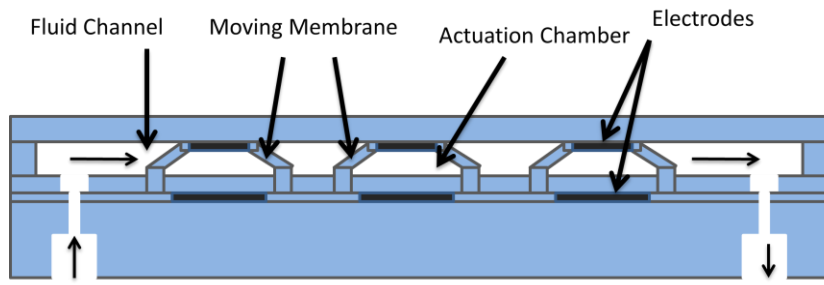


FIG 3-2 – Schematic of the peristaltic micropump

References

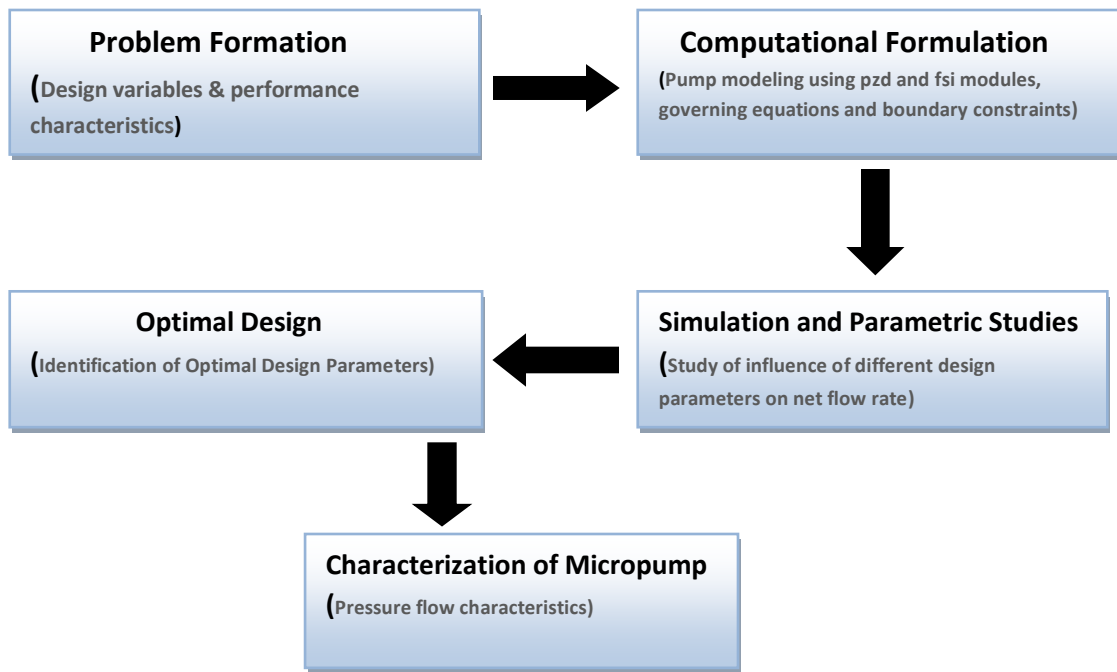
- [1] Soderstrom RM. Injuries to major blood vessels during endoscopy. *J Am Assoc Gynecol Laparosc*. 1997 May;4(3):395-8. doi: 10.1016/s1074-3804(05)80234-8. PMID: 9154792.
- [2] Villa, Edward et al. “Endoscopy-related musculoskeletal injuries in gastroenterology fellows.” *Endoscopy international open* vol. 7,6 (2019): E808-E812. doi:10.1055/a-0811-5985

Chapter 4

Simulation and Results

4.1 Nozzle/Diffuser Micropump for NPWT.

Simulations are carried out to find optimal design parameters for the valveless micropump. In this study, the effect of the principle dimensions of the diffuser element including diffuser angle, diffuser length, neck width, and thickness of diaphragm on the micropump characteristics such as flow rate and back pressure is analyzed. The process flow of the work is as follows-



For the simulation, we have used COMSOL Multiphysics 5.5.

COMSOL Multiphysics

COMSOL Multiphysics is a cross-platform finite element analysis, solver and Multiphysics simulation software which allows conventional physics-based user interfaces and coupled system

of partial differential equations (PDEs). COMSOL provides an IDE and unified workflow of electrical, mechanical, fluid, acoustics and chemical applications.

Beside the classical problems that can be addressed with application modules, the core Multiphysics package can be used to solve PDEs in weak form. It contains advanced numerical routines to handle challenging peculiarities such as periodic boundary conditions, average value constraints, and adaptive grid mesh refinement procedures.

4.1.1 Design and Geometry

The micropump was designed in COMSOL Multiphysics. For the simulation two modules were used- Fluid Structure Interaction Module and the Piezoelectric Module. The micropump was designed following the theoretical consideration described in Chapter 2. The pump consisted of two diffuser elements, fluid chamber, PDMS membrane, brass diaphragm and the piezoelectric disc on the top. To have a fully developed inlet and outlet constriction channels were also included in the geometry along with round inlet and outlet.

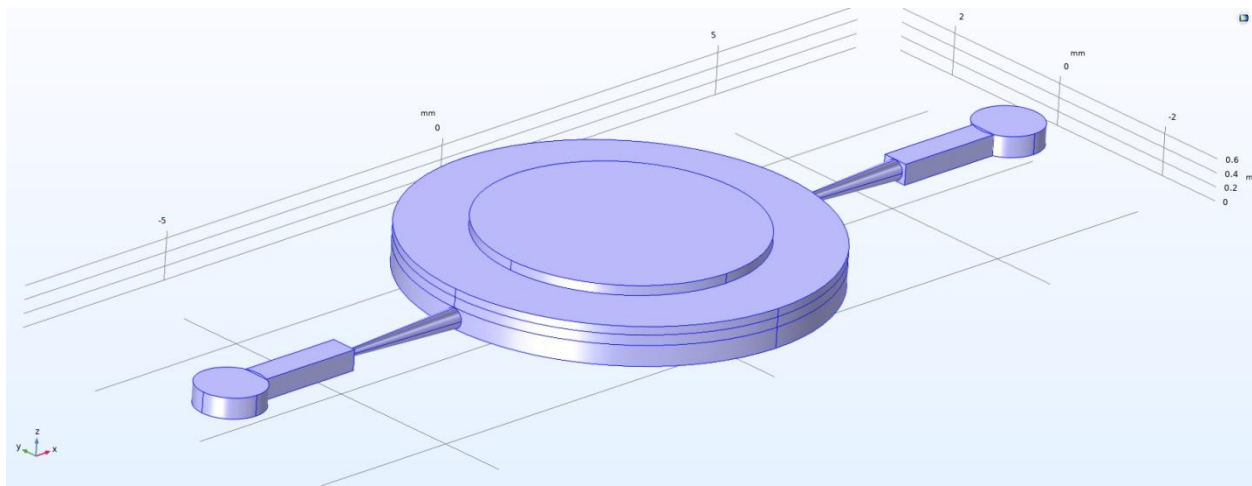
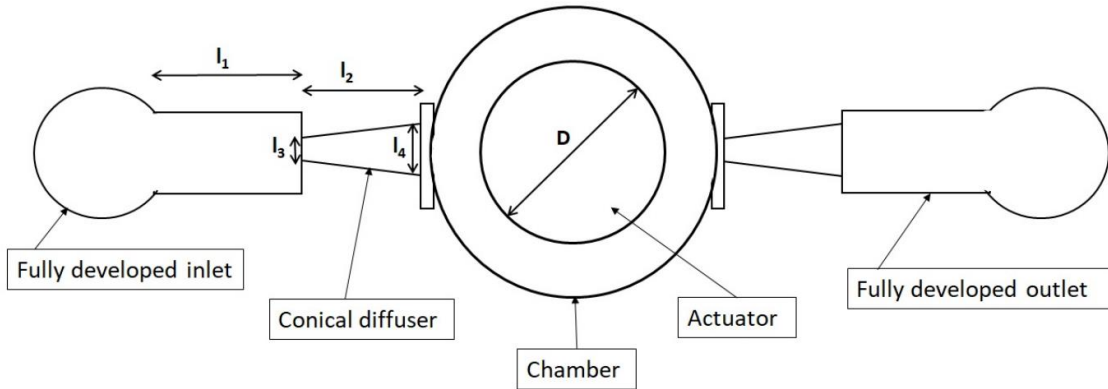


FIG 4-1 – Design of the nozzle/diffuser micropump for NPWT



The parameters of the micropump of Fig 3-1 is as follows.

| Description | Expression | Value |
|--------------------------------------|-------------------|--------------|
| Radius of the Chamber | 3 [mm] | 0.003 m |
| Height of the chamber | 300 [um] | 3E-4 m |
| Diffuser Length | 1.1[mm] | 1.1E-3 m |
| Diffuser Height | 300 [um] | 3E-4 m |
| Neck width (l_3) | 100 [um] | 1E-4 m |
| Neck width (l_4) | 180 [um] | 1.8E-4 m |
| Constriction channel | 1.6 [mm] | 0.0016 m |
| length(l_1) | | |
| Constriction channel width | 400 [um] | 4E-4 m |
| Constriction channel height | 300 [um] | 3E-4 m |
| Membrane Radius | 3 [mm] | 0.003 m |
| Membrane Height | 150 [um] | 1.5E-4 m |
| Brass Radius | 3 [mm] | 0.003 m |
| Height of Brass | 120 [um] | 1.2E-4 m |
| Radius of Piezoelectric layer | 2 [mm] | 0.002 m |
| Piezoelectric layer height | 140 [um] | 1.4E-4 m |
| Applied Voltage | 50 [V] | 50 V |
| Frequency of actuation | 60 [Hz] | 60 Hz |
| Boundary Stress (high) | 1e4 | 10000 |
| Boundary Stress (low) | 1e-1 | 0.1 |
| Inlet Radius | 0.5[mm] | 5E-4 m |
| Outlet Radius | 0.5[mm] | 5E-4 m |
| Height of inlet channel | 300 [um] | 3E-4 m |
| Height of outlet channel | 300 [um] | 3E-4 m |

| Component/Material | Parameter/variable | Value | Unit |
|-------------------------------|---------------------|-------|------|
| Piezoelectric Actuator | Alternating Voltage | 50 | V |
| | Actuation Frequency | 60 | Hz |

4.1.2 Boundary Conditions

For boundary conditions, fixed and zero displacement boundary conditions were applied at the edges of the diaphragm. To ensure no or zero relative motion at the interface between the diaphragm, brass disc and the PZT element the “always bonded” boundary condition was given. The fixed boundary is shown in Fig 4-2.

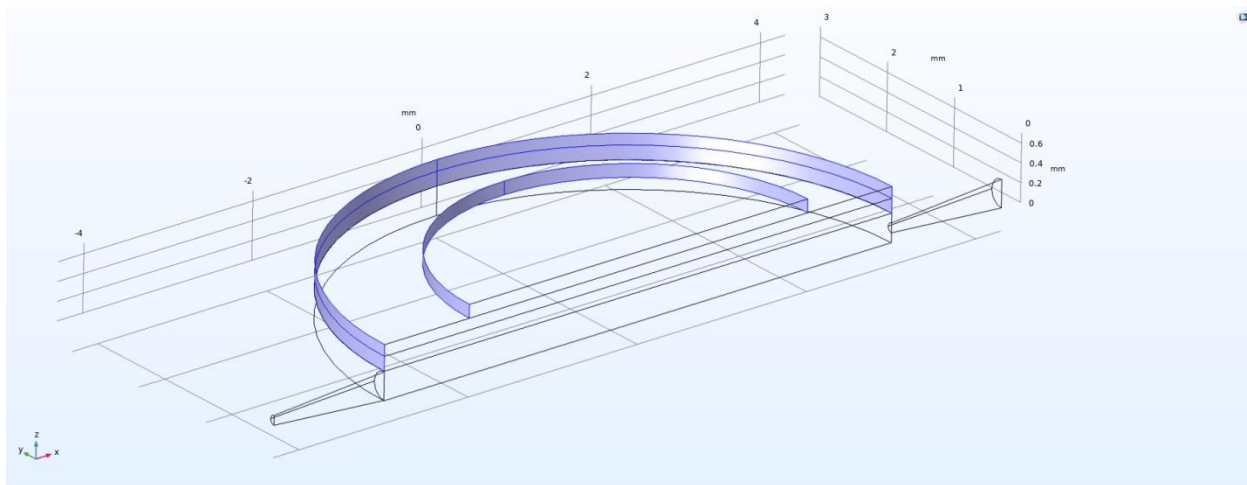


FIG 4-2 – Fixed boundaries at the edges of the diaphragm, brass disc and Piezo disc.

A symmetry plane was applied to the whole micropump geometry (Fig 4-1). This symmetry/work plane is shown in Fig 4-3.

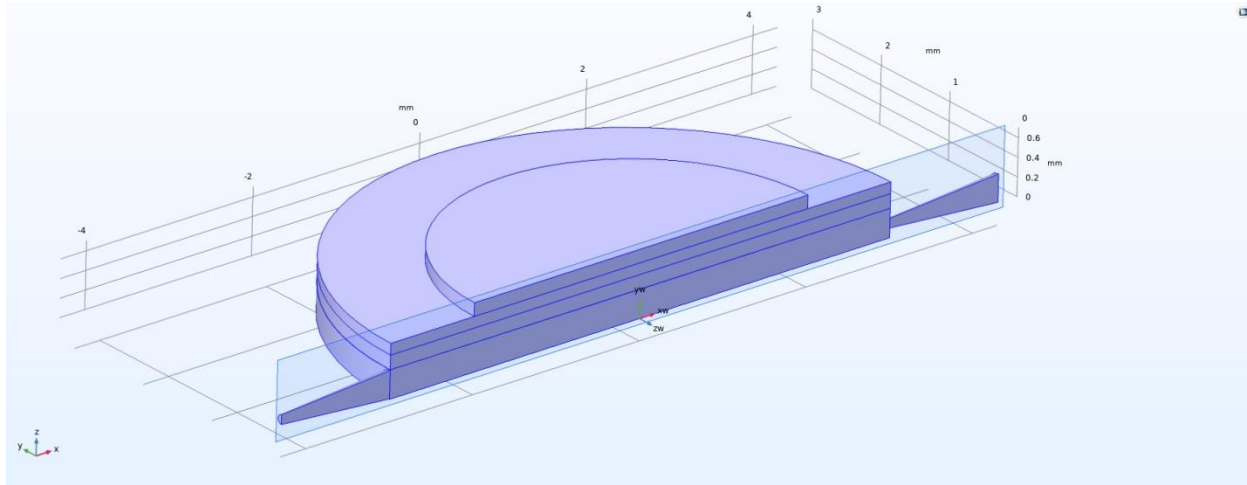


FIG 4-3 Symmetry/Work Plane of the Micropump

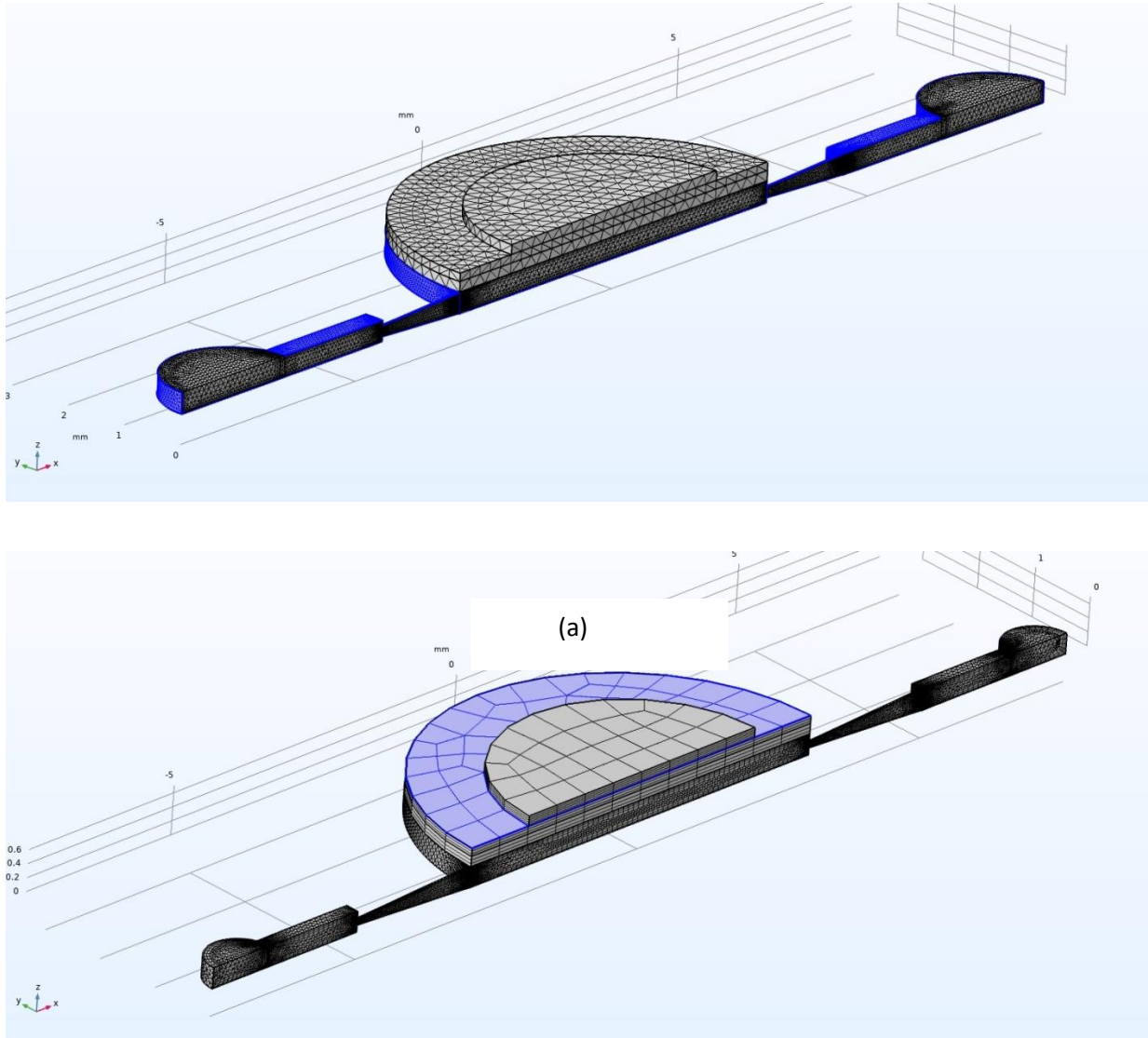
For inlet/outlet boundary condition, the inlet and outlet work by employing check valves to ensure a one-way flow. In the model the valve is represented by a simple boundary condition based on K-factor piping losses, where the losses are high when flowing against the valve and low when flowing in the direction of operation. The back pressure resulting from the valve is represented by the following equation:

$$p = A\rho u_{av}^2 \quad (4.1)$$

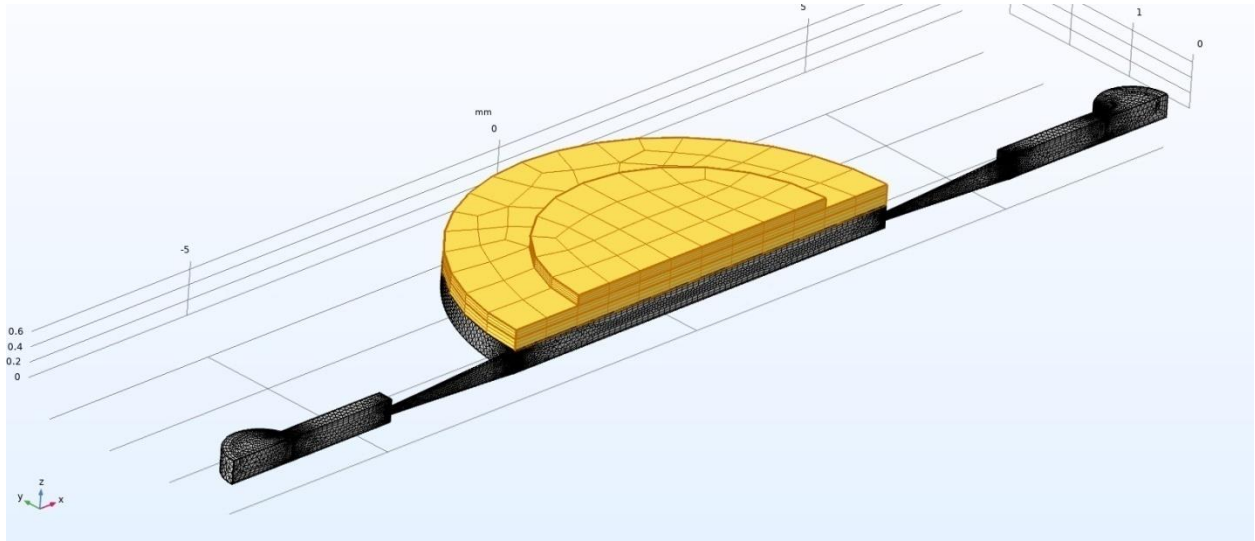
Where, u_{av} is the average velocity of the fluid normal to the boundary, ρ is the fluid density and A is a dimensionless constant that changes magnitude depending on the sign of u_{av} . The back pressure is applied as a normal stress at the end of a short length of pipe - which ensures that the fluid flow in the domain is realistic, despite this approximate boundary condition. This boundary condition can be employed to represent a simple fluid valve or diode. The constants used for the outlet boundary are reversed with respect to those used in the inlet, representing a different orientation of a similar valve. This encourages flow through the pump in the desired direction. To represent a low resistance valve (such as a simple flapper valve), set A to 5,000 for closed condition and to 0.1 for the open condition.

4.1.3 Mesh Formation

To save computation time for the purposes of this example, a relatively coarse mesh is used. Different types of meshing have been employed to best define the structure. For this Quad Mesh, Swept Mesh, Boundary Layers have been used. The formed mesh is shown in Fig 3-4.



(b)



(c)

FIG 4-4 – (a) The mesh used in the model. **Note** the fluid boundary layers next to the highlighted fluid walls. (b) Quad Mesh (c) Swept Mesh

FIXED and VARIABLE PARAMETERS

In the model above, to find the optimal geometry for the blood flow, some parameters of the geometry were kept fixed while some were changed. The fixed parameters for the micropump above are-

1. Fluid Chamber Diameter
2. Fluid Chamber Depth
3. Diaphragm Diameter
4. Diaphragm Thickness
5. Brass Diameter
6. Brass Thickness
7. PZT Diameter
8. PZT Thickness.

The parameters which were varied in the micropump were-

1. Diffuser Length
2. Diffuser Angle

Studies were also conducted for different fluids- Water, Ethanol, Blood Plasma. But, to find the optimal geometry, blood plasma has been used.

It was seen that for diffuser length 1.1mm and diffuser angle 9°, the max flow rate was obtained.

4.2 Results

Piezoelectric Actuation

As per the piezoelectric effect after application of the voltage on the piezoelectric disc the deformation of the disc was seen as shown in Fig 4-5. A study of how the bending increases with increasing applied voltage was also gathered as shown in Fig 4-6.

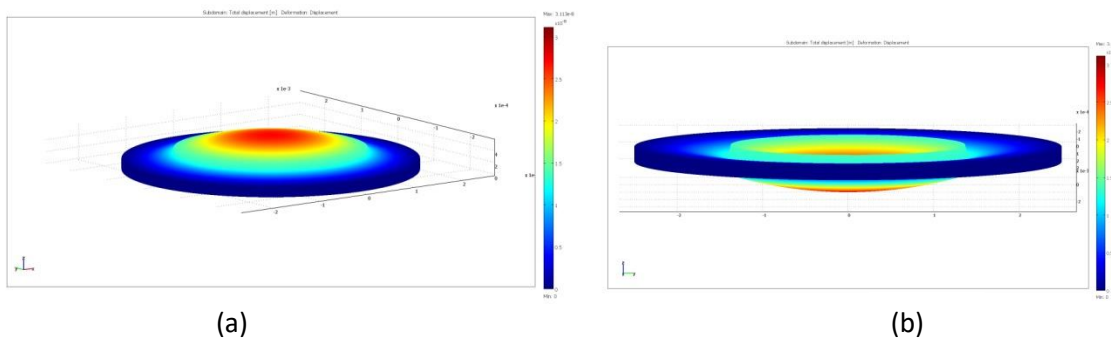


FIG 4-5 Deformation of the piezoelectric actuator with applied voltage

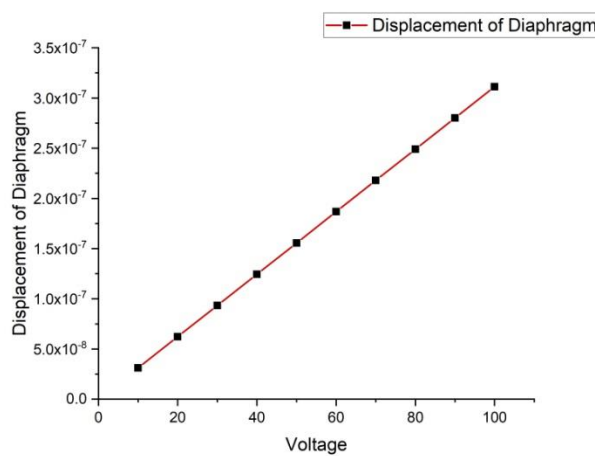


FIG 4-6 Displacement of the Diaphragm with applied voltage

Plots for different changes in diffuser length and diffuser angle have been computed. The diffuser length has been varied from 0.9mm – 1.5mm along with that the diffuser angle has also been varied from 5° - 11° .

Diffuser Length -1.1mm, Diffuser angle- 9°

The following geometry was computed for blood plasma.

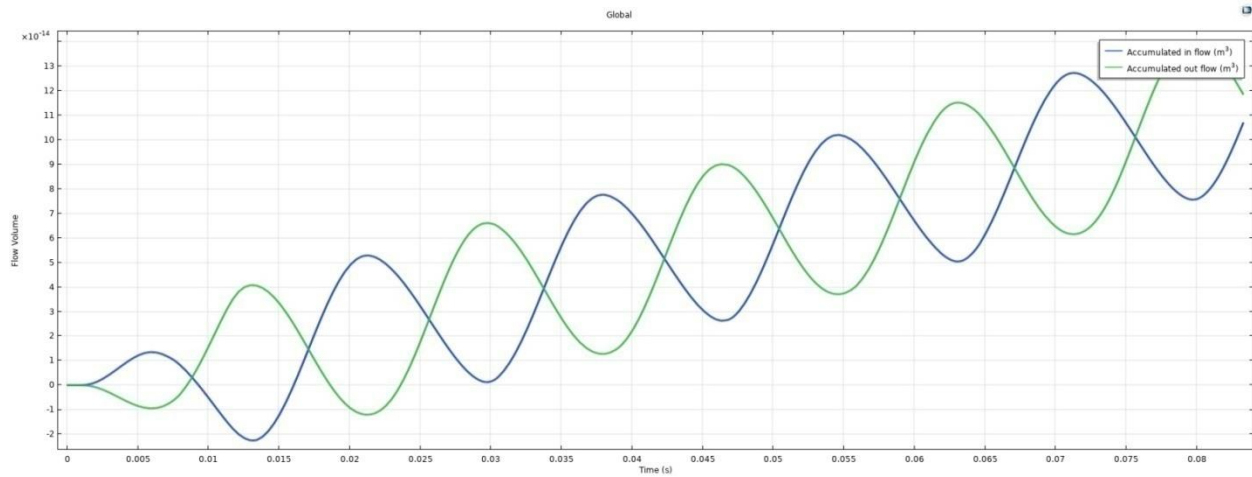
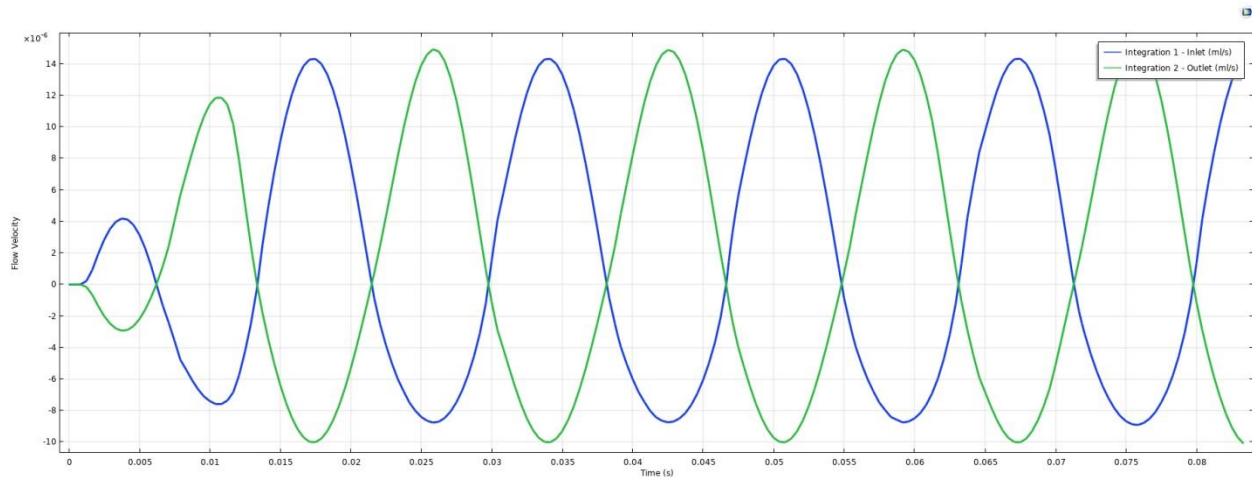


FIG 4-7- Net fluid flow through the inlet and the outlet over time, computed using a global ordinary differential equation.

The accumulated flow for blood plasma has been plotted. The time integrated flows into the inlet and out of the outlet are calculated using a global ODE and are shown in Fig 4-7.



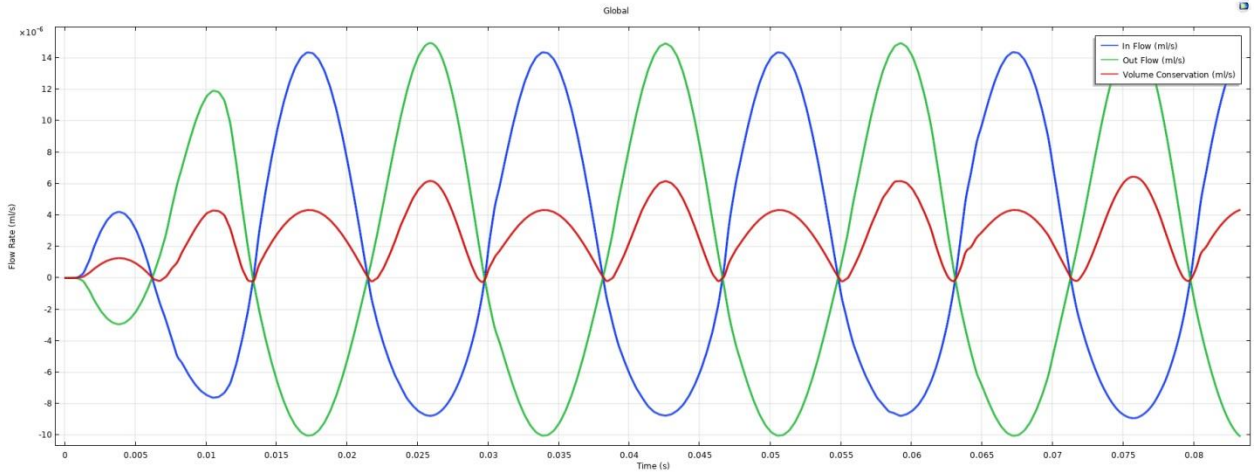
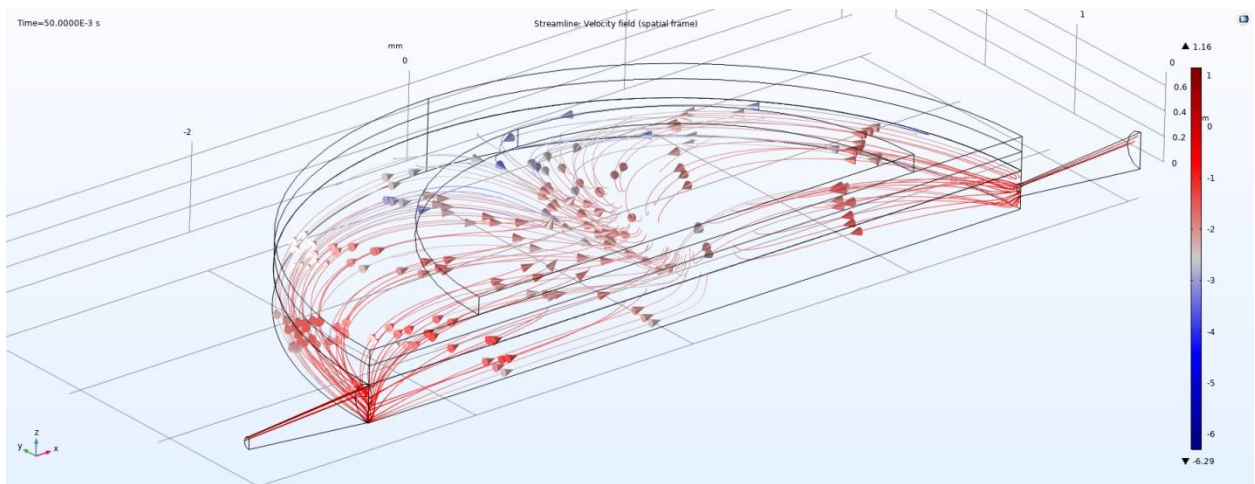


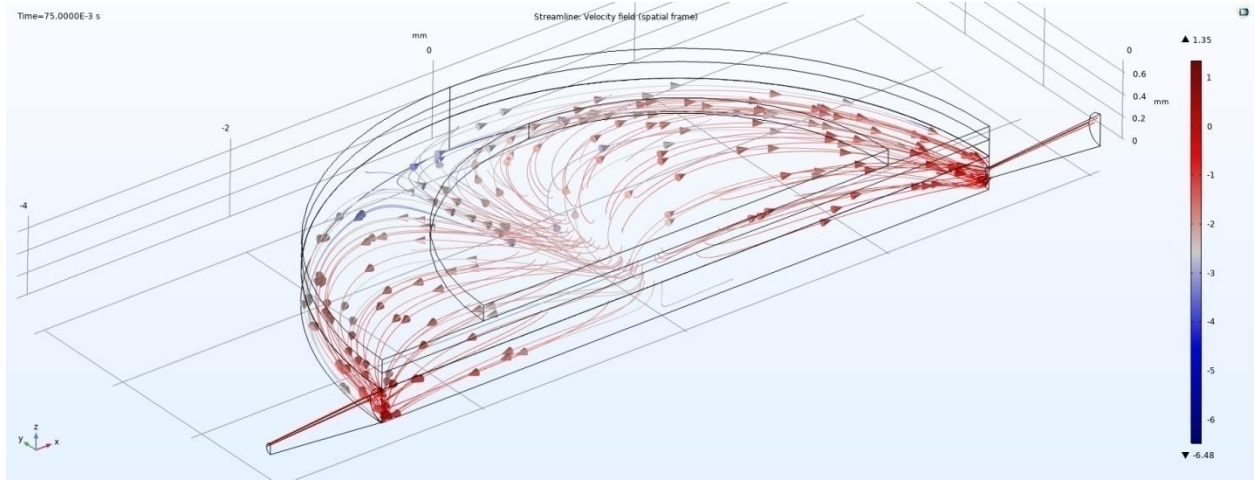
FIG 4-8 - *Flow rates and volume conservation.*

Fig 4-8 shows the inlet and outlet flow rates and confirms the conservation of fluid volume within the device. The drive voltage is ramped up during the first 3/4 of the actuation period. Afterward, a consistent time periodic flow is quickly established. The difference in inlet and outlet flow matches the volume of the fluid displaced by the membrane due to the piezoelectric stroke, confirming the volume conservation.

The fluid streamlines for the inflow and outflow can be seen in Fig 4-9. The inflow can be seen at a time of 0.05s and the outflow can be seen at 0.075s. This is in accordance with the piezoelectric actuation frequency of 60 Hz.



(a)



(b)

FIG 4-9- (a) Fluid Streamline during inflow at time $t= 0.05s$ (b) Fluid streamlines during outflow at time $t= 0.075s$

For the piezoelectric actuation, after deformation, the Von-Mises Stress was also plotted in Fig 4 -10.

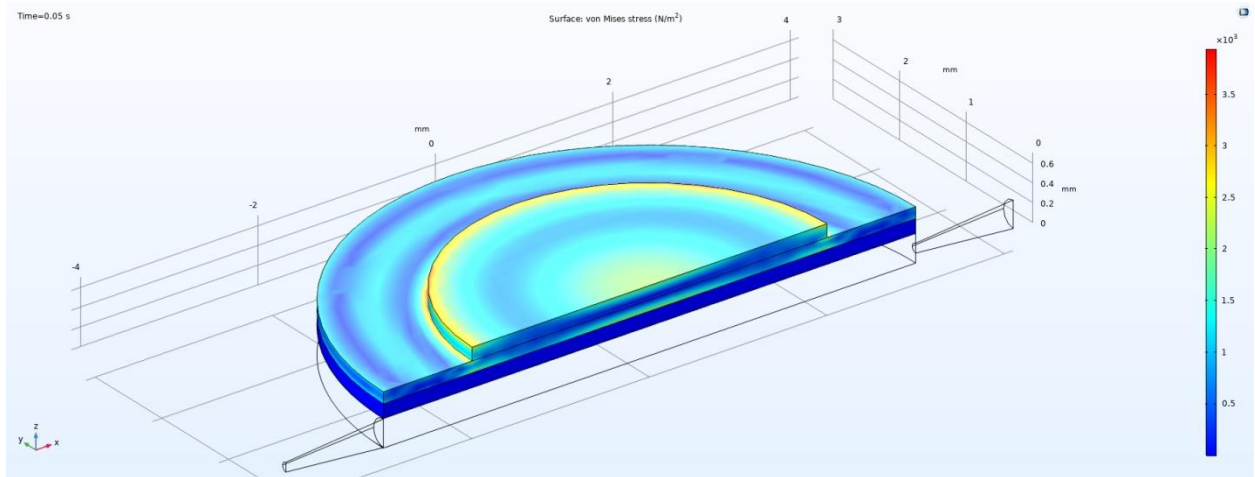
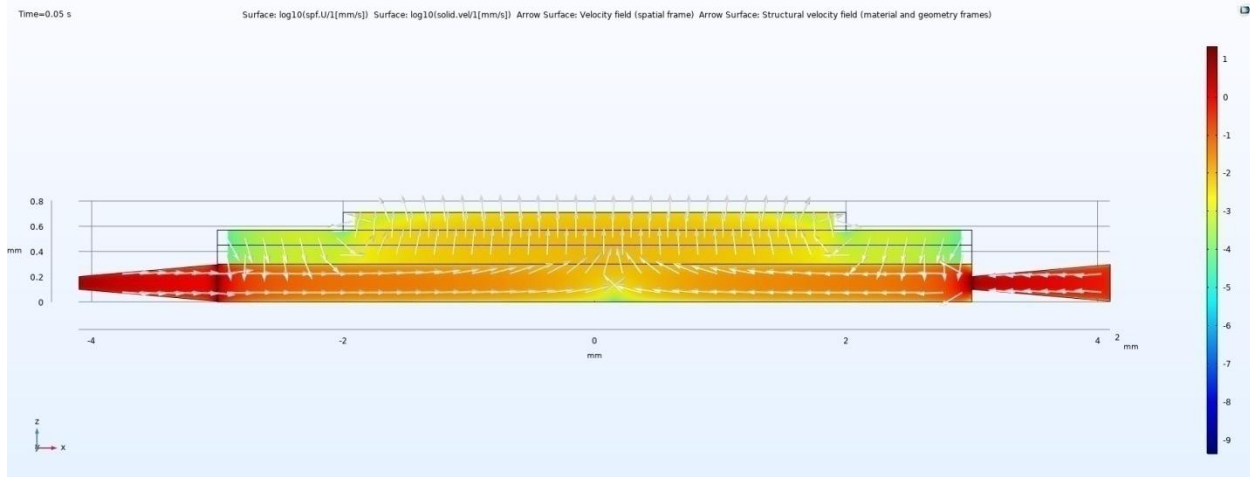
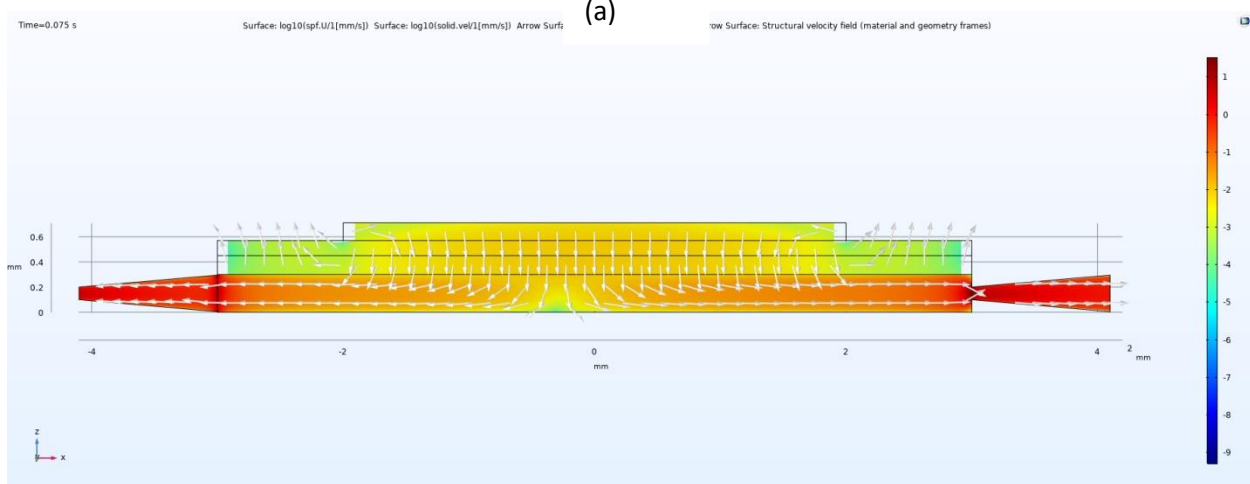


FIG 4-10 – von-Mises Stress after piezoelectric actuation at time $t= 0.05s$



(a)



(b)

FIG 4-11 (a) Velocity Field of the micropump at time $t=0.05\text{s}$ (b) time $t=0.075\text{s}$

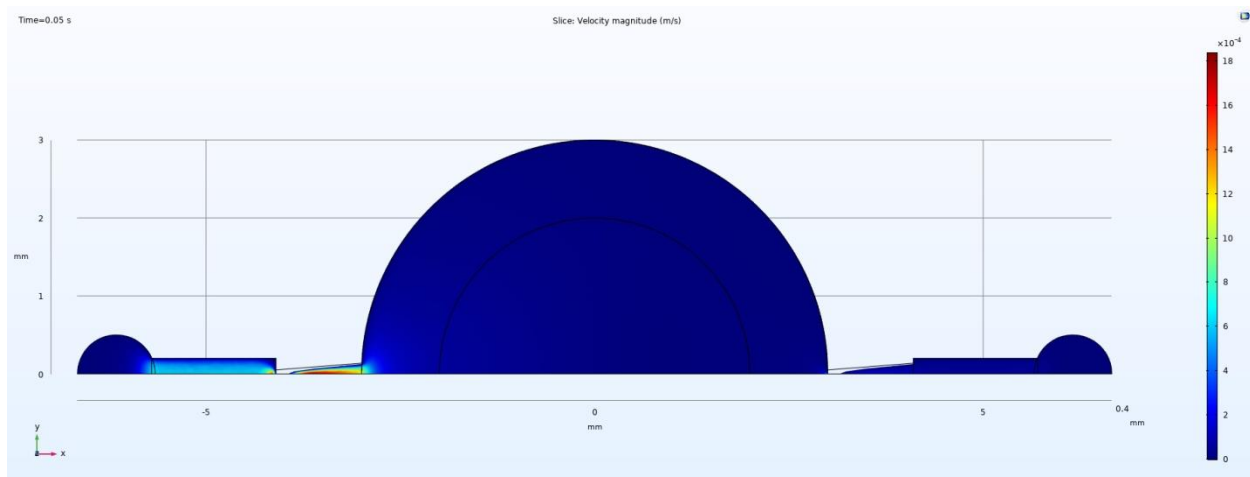


FIG 4-12 Fluid Velocity magnitude during Inflow

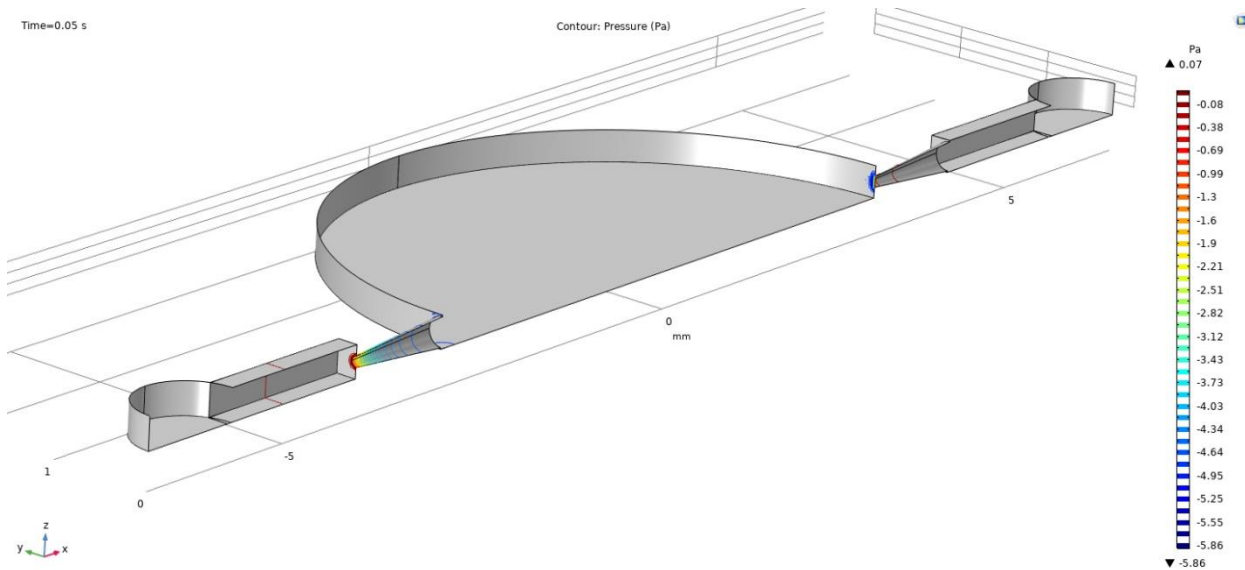


FIG 4-13 Liquid Pressure at $t = 0.05s$

The flow characteristics of the pump were compared to other geometry with changing Diffuser Length.

Now, the optimal geometry of the pump was simulated for three different liquids- water, ethanol, blood plasma.

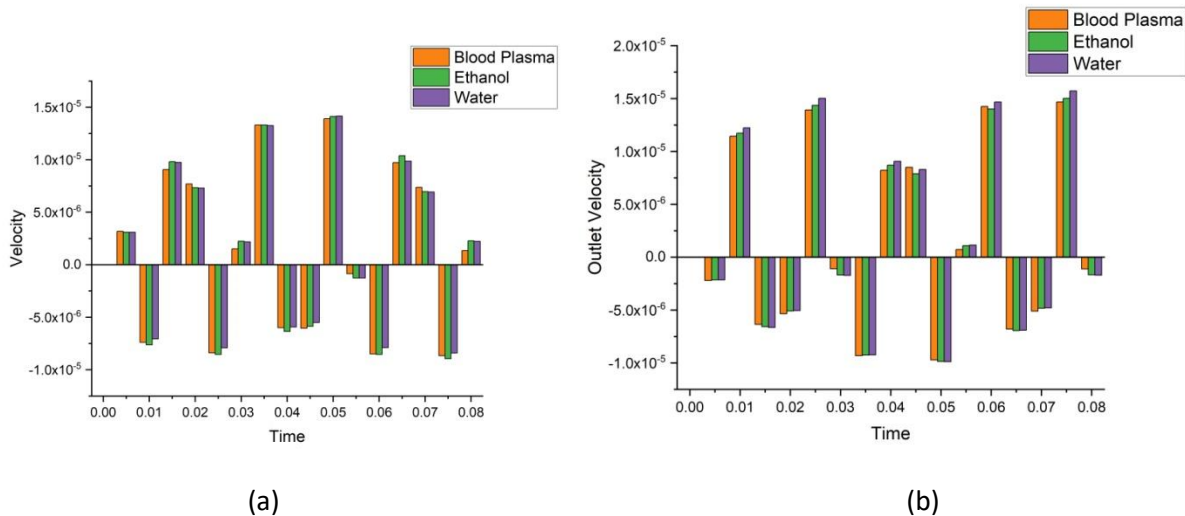


FIG 4-14 Comparison of (a) Inlet (b)Outlet velocities for different fluids- Blood Plasma, Ethanol, Water

Comparison of Micropump Geometries

The diffuser length of the micropump has been varied from 0.9mm to 1.5mm. The accumulated volume of such micropumps was computed along with the inlet/outlet flow rate. Individual graphs of the micropump are plotted as follows.

Diffuser Length- 0.9mm

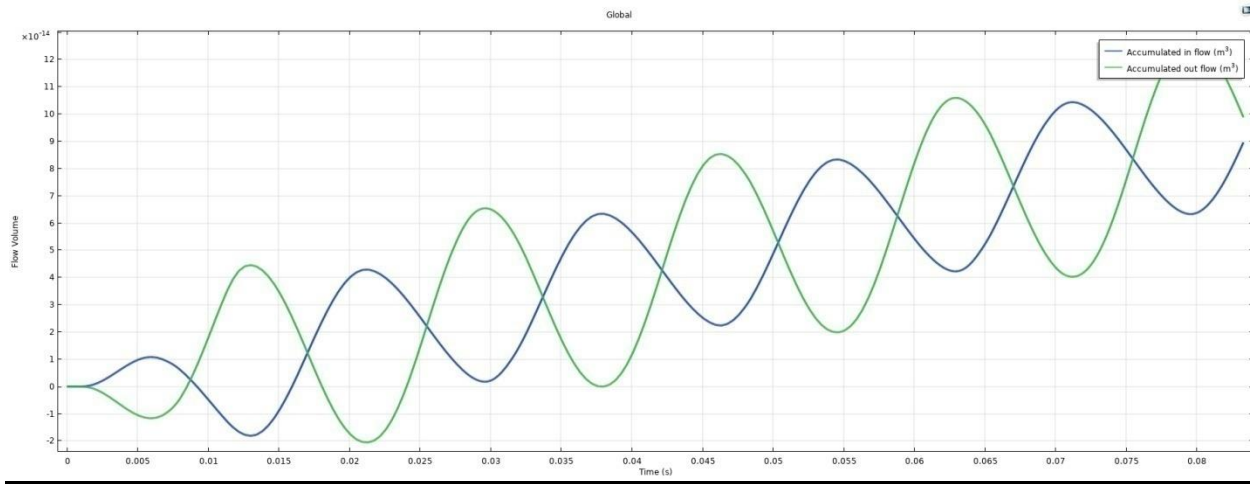


FIG 4-15- *Accumulated Flow Volume with diffuser length 0.9mm*

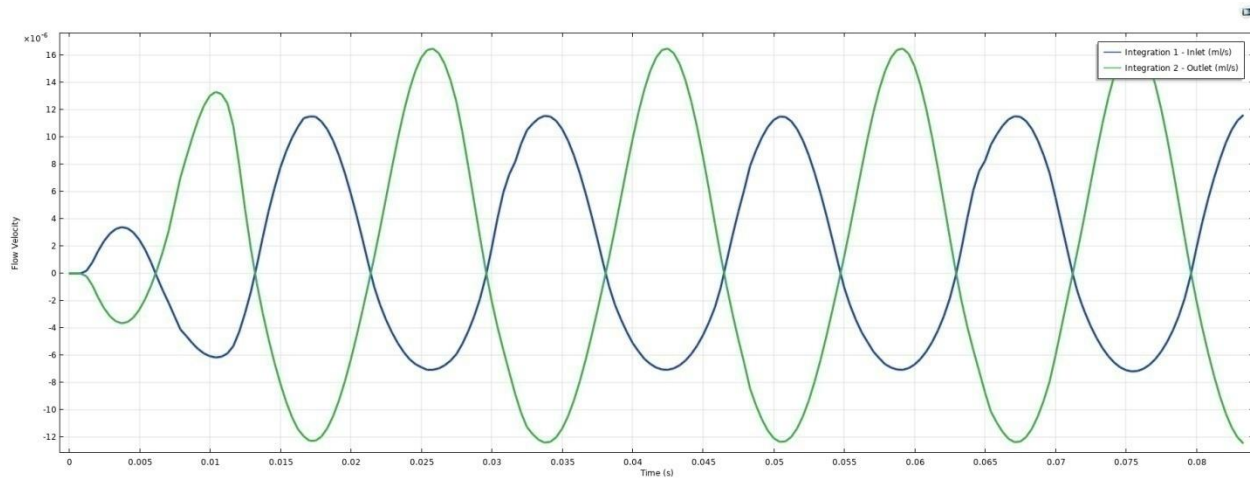


FIG 4-16- *Flow velocity from Inlet/Outlet for diffuser length 0.9mm*

Here, it can be seen that the inlet velocity at all times is lesser than the outlet velocity which does not serve the alternating increase in inlet and outlet velocity. Thus, this is not the optimal case.

Diffuser length - 1.1mm

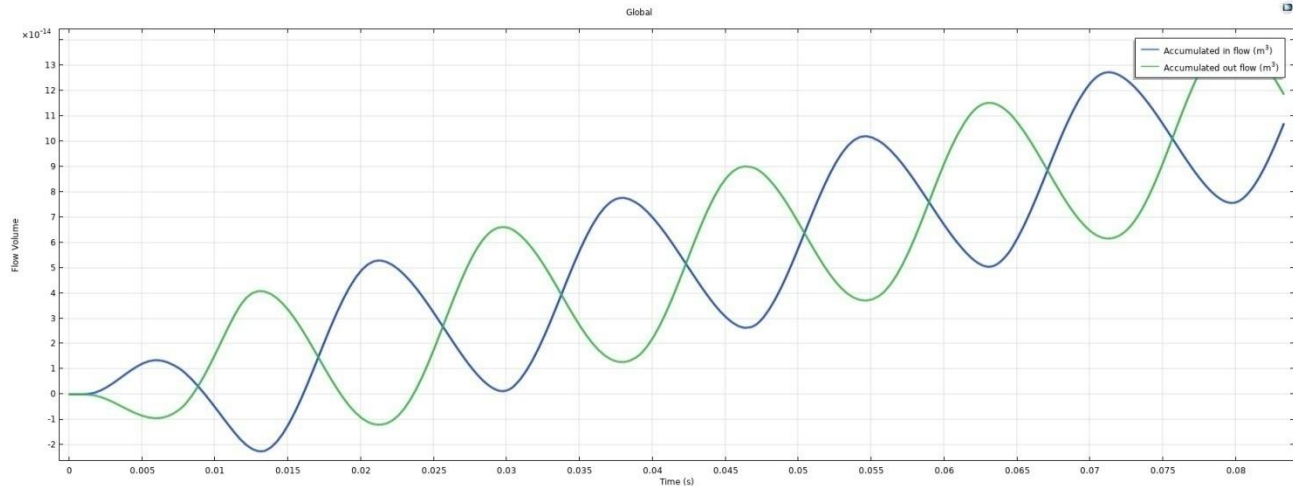


FIG 4-17- Accumulated Flow Volume for diffuser length 1.1mm

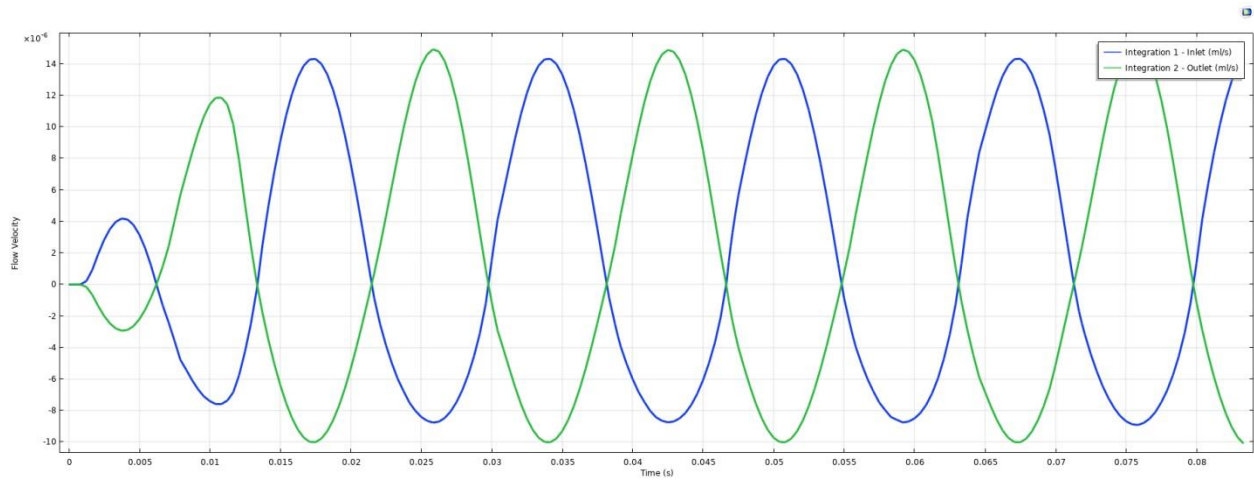


FIG 4-18- Flow velocity of Inlet/Outlet for diffuser length 1.1mm

Here, it can be seen that the inlet/outlet velocity follows the alternating high and low velocity pattern which serves as the optimal case.

Diffuser length - 1.3mm

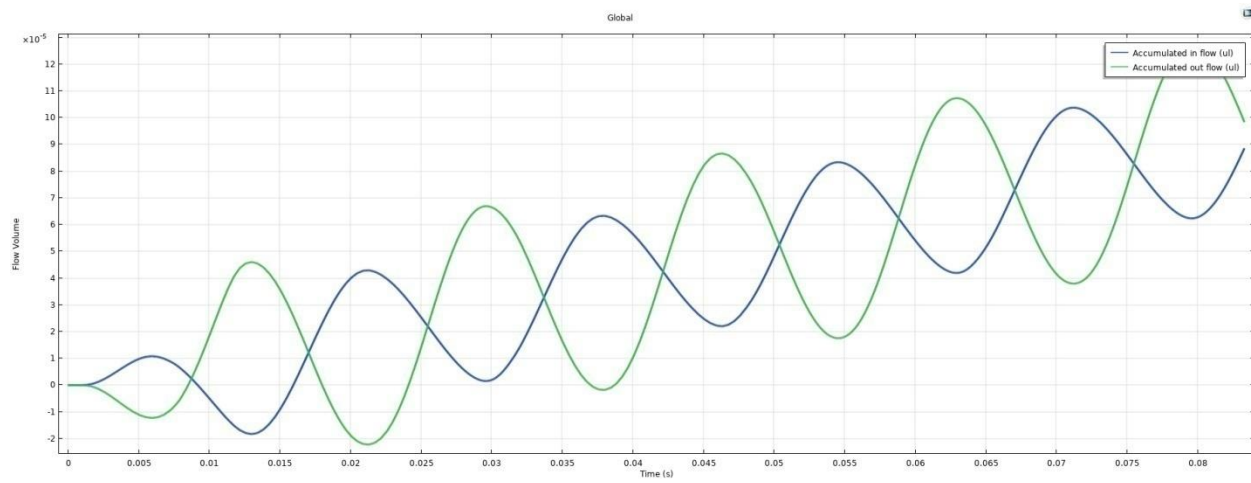


FIG 4-19- *Accumulated Flow Volume for diffuser length 1.3mm*

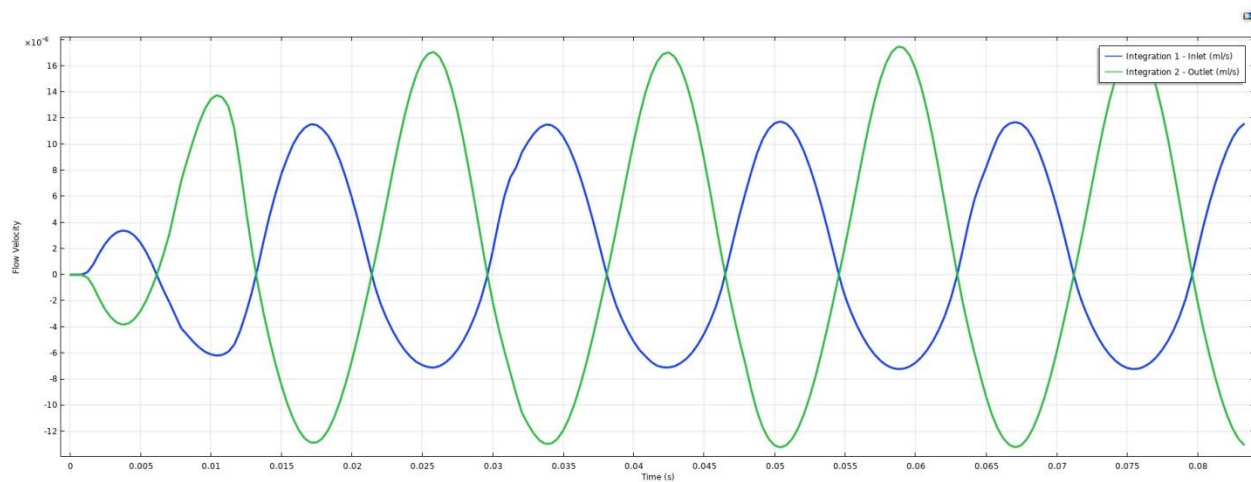


FIG 4-20- *Flow velocity of Inlet/Outlet for diffuser length 1.3mm*

Here, again the outlet velocity is higher than inlet velocity all the time was again not the favorable case for micropump.

Diffuser length - 1.5mm

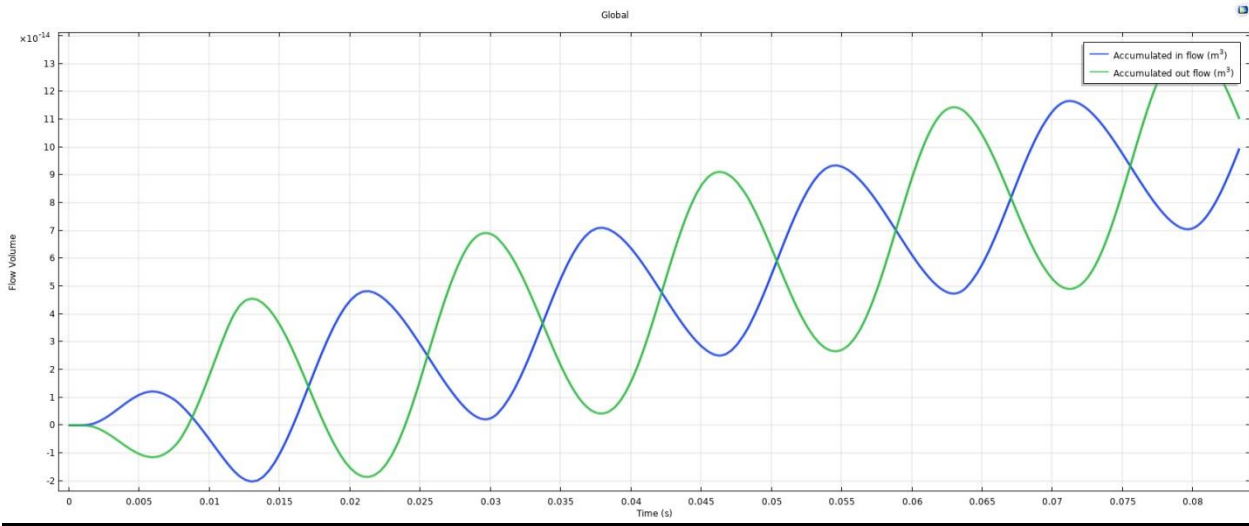


FIG 4-21- *Accumulated Flow Volume for diffuser length 1.5mm*

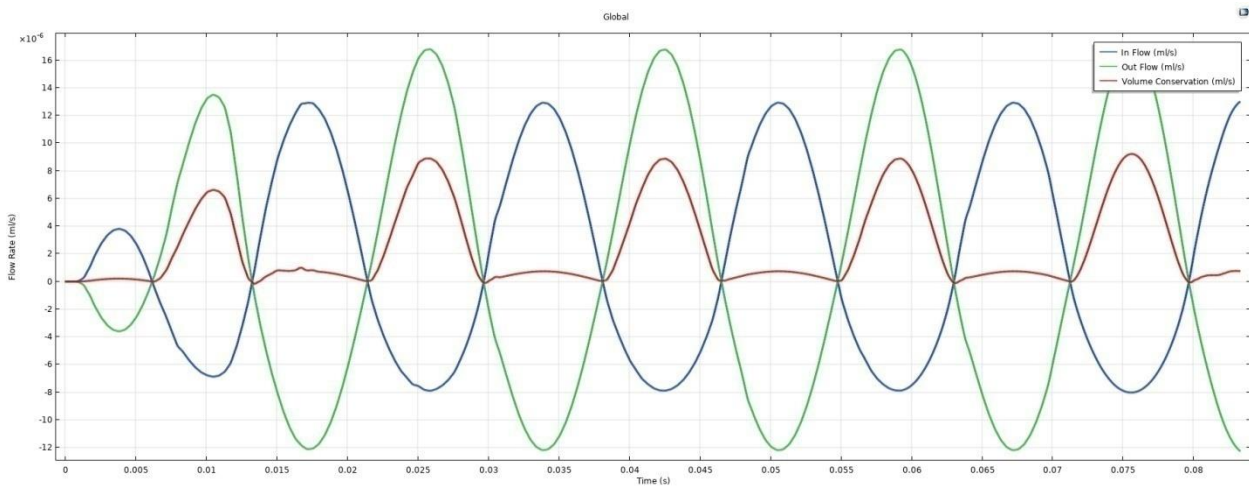


FIG 4-22- *Flow velocity of Inlet/Outlet for diffuser length 1.5mm*

Here, though the alternating phenomenon is seen, the difference between the inlet and the outlet flow rate is less which affects the accumulated flow volume.

Thus, from the above study, it was seen that a diffuser length of 1.1mm serves as the best for maximum flow rate of fluid.

Note: The fluid which is used in the above simulation is Blood Plasma.

Now, the diffuser angle of the micropump was changed so to obtain the optimum geometry for the fluid flow.

Diffuser angle - 8°

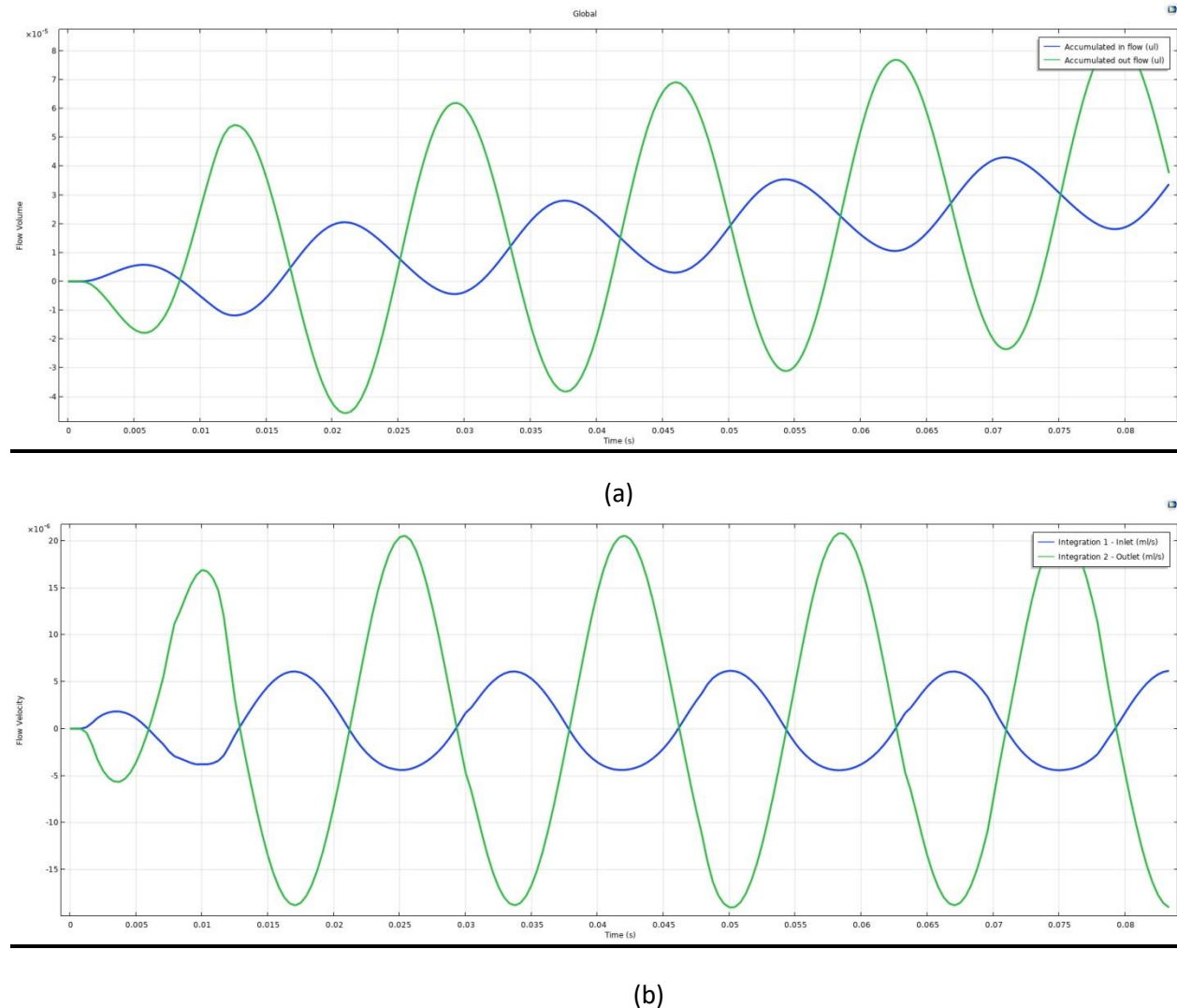
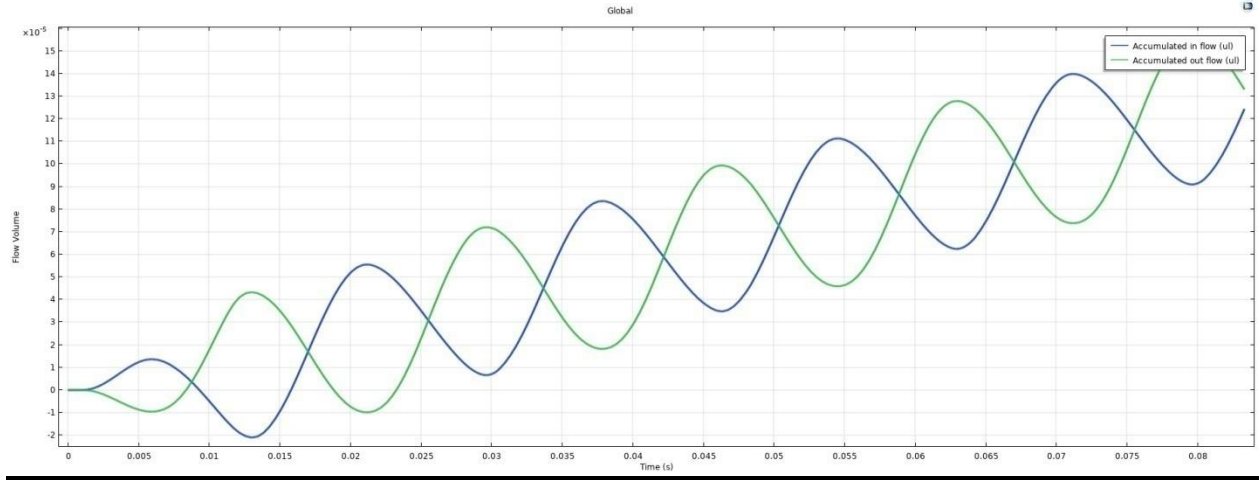
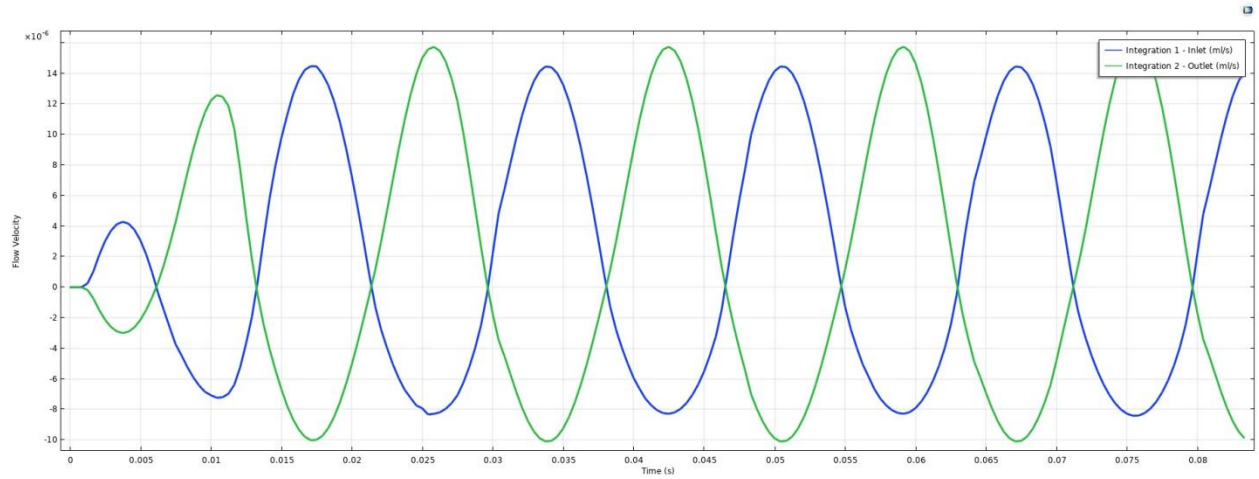


FIG 4-23 (a) Accumulated Flow Volume for diffuser angle 8° (b) Flow velocity of Inlet/Outlet for diffuser angle 8°



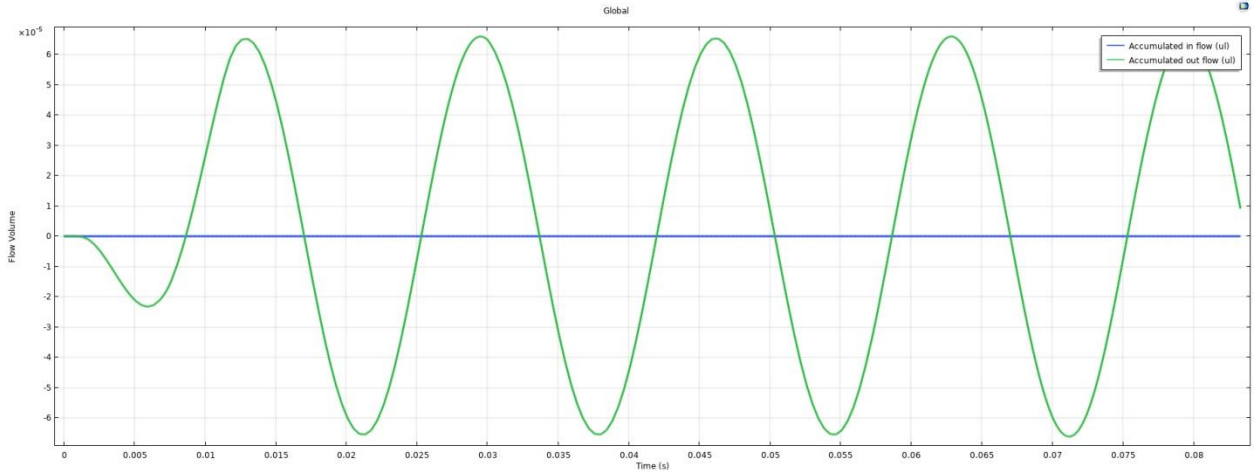
(a)



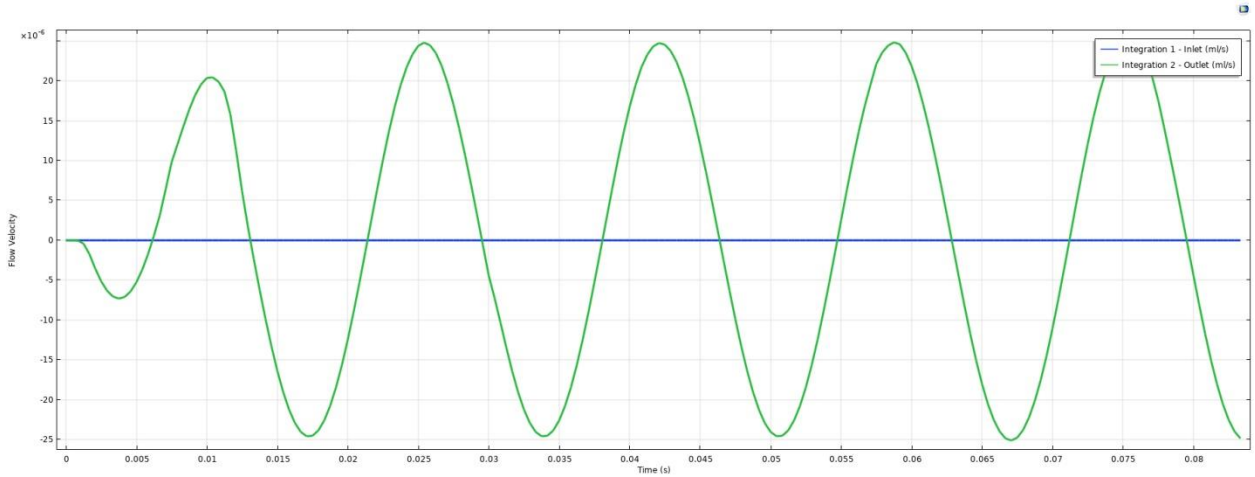
(b)

FIG 4-24 (a) Accumulated Flow Volume for diffuser angle 9° (b) Flow velocity of Inlet/Outlet for diffuser angle 9°

\



(a)



(b)

FIG 4-25 (a) Accumulated Flow Volume for diffuser angle 10° (b) Flow velocity of Inlet/Outlet for diffuser angle 10°

From the above plots for different diffuser angles, it can be seen that the maximum increase in the flow rate was observed for the diffuser angle 9° . Thus, the optimal geometry for the fluid flow in the conical diffuser was observed at a diffuser length of 1.1mm and angle of 9° .

4.3 Design of Peristaltic Micropump

The micropump was designed in COMSOL Multiphysics. For the simulation two modules were used- Electromechanics Module which couples electrostatic with solid mechanics and interaction of both and Fluid Flow model. In the Fluid flow model, Laminar Flow in Single Phase Flow was selected. The pump designed was of dimensions- 3mm x 0.25mm. This pump is made for the application of pumping liquid from inside the eye. Thus, miniature size was a must. The design of the pump is shown below in Fig. 4-23.

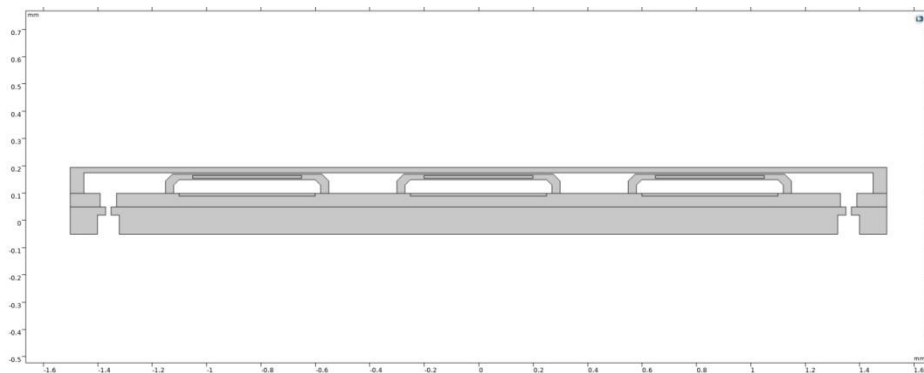


FIG 4-26- Schematic of the Peristaltic Micropump

Following the theoretical pumping cell model, the micropump was designed to have three movable membranes with Au electrodes.

Principle of Operation

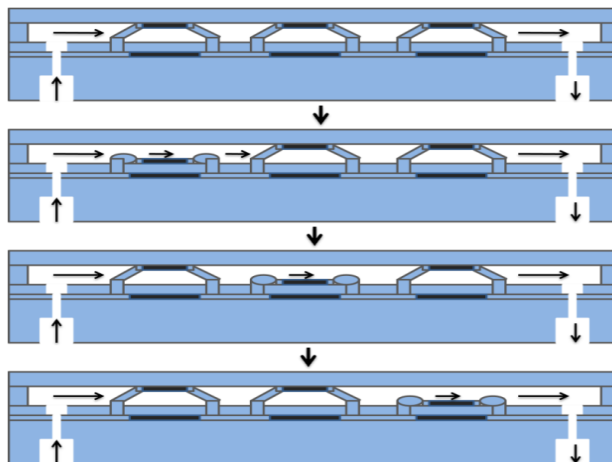


FIG 4-27 - Principle of Operation of the peristaltic Micropump

5. Summary and Conclusion

In this study, we have designed and simulated micropumps for the treatment of two medical diseases- treatment of Wound, treatment of Glaucoma. The MEMS nozzle/diffuser micropump was used for NPWT. Comparison of different geometries was done to find the optimal figure for efficient pumping. The modeling used pressure inlet/outlet conditions to have unidirectional flow of fluid. It is well-intentioned that the micropump performance characteristics namely flow rate and back pressure are predominately influenced by geometrical parameters as well as operating conditions. The micropumps' performance can be enhanced through proper choice of geometrical and operating conditions.

Based on the extensive simulations performed in this study, the following conclusions are drawn which highlight the findings in respect of proposed piezoelectric actuation based valveless micropump:

- Simulation results of velocity vectors at diffuser/nozzle configuration show that the flow entering into the pump chamber through the inlet during the supply mode is more as compared to the flow exiting the inlet during the pump mode. This represents flow rectification property of the nozzle/diffuser elements.
- In a nutshell, it is clear that the micropump performance is affected by principal dimensions of nozzle/ diffuser, pump chamber dimensions and diaphragm dimensions. There are certain threshold values of these parameters which are required for desired performance.
- The dimensions of optimal diffuser/nozzle geometry are divergence angle = 9° , diffuser length = 1.1 mm and neck width = 0.100 mm. The optimal chamber depth is found to be 300 μm .
- Variation in flow rates have been observed for different fluids- Water, Ethanol, Blood Plasma.

For the treatment of Glaucoma, the concept of the device was introduced. Self-actuating design of the micropump was seen with integrated piezoelectric pressure sensor which serves

as the actuator to initiate the working of the micropump. The peristaltic pump was designed to have dimensions of 3mm x 0.25mm.

6. Future Scope

The fabrication and integration of both the devices is to be done. The application of the devices in real life becomes the most important factors. Comparison of results from simulation and experimental devices is to be done for real life applications. These devices can prove very helpful for the treatment of wound and especially glaucoma. Several drug deliveries through MEMS micropumps have been done earlier, though no such permanent solution was seen. The fabricated pump will serve as an easy solution to such chronic diseases.